JAERI-Research
96-016

THE BIAXIAL STRENGTH AND FRACTURE CRITERIA FOR HTGR GRAPHITES

March 1996

Motokuni ETO, Shintaro ISHIYAMA
T.D. BURCHELL* and G.T. YAHR*

日本原子力研究所
Japan Atomic Energy Research Institute

本レポートは，日本原子力研究所が不定期に公刊している研究報告書です。
入手の問合わせは，日本原子力研究所技術情報部情報資料課（〒319-11 茨城県那珂郡東海村）あて，お申し越しください。なお，このほかに財団法人原子力弘済会資料センター（〒319-11 茨城県那珂郡東海村日本原子力研究所内）で複写による実費頒布をおこなっております。

This report is issued irregularly.
Inquiries about availability of the reports should be addressed to Information Division, Department of Technical Information, Japan Atomic Energy Research Institute, Tokai-mura, Naka-gun, Ibaraki-ken 319-11, Japan.

編集兼発行　日本原子力研究所
印　　刷　㈱原子力資料サービス

THe Biaxial Strength and Fracture Criteria for HTGR Graphites

Motokuni ETO, Shintaro ISHIYAMA, T.D. BURCHELL*
and G.T. YAHR*

Department of High Temperature Engineering
Tokai Research Establishment
Japan Atomic Energy Research Institute
Tokai-mura, Naka-gun, Ibaraki-ken

(Received February 21, 1996)

The strength and fracture criteria at the biaxial stress state were examined for two grades of HTGR graphites, i.e., a fine-grained isotropic IG-11 and a medium-grained semi-isotropic PGX. The biaxial stress state was realized using a servohydraulic testing machine in combination with an apparatus for applying the internal pressure or the torque force to a tubular specimen. Three kinds of specimens were tested at room temperature: (1) the larger specimens with different wall thicknesses (2 to 20 mm) to make clear the effect of wall thickness on the biaxial strength, (2) the smaller ones with wall thickness of 2 mm to obtain data for the statistical analysis, and (3) specimens tested at ORNL to examine if there is any discrepancy in the strength data which may result from the differences in the rig and specimen size.

Main results are: (1) As for the failure surface no significant effect of wall thickness was observed though the number of the specimens tested was not large enough to evaluate the data statistically. (2) On the basis of the statistical analysis of the data on the smaller IG-11 specimens, the modified maximum strain energy criterion gave the best fit to the data points both in the first and fourth quadrants of the fracture surface. (3) The data obtained at ORNL fell on the scatter band of the JAERI data, which indicated that no appreciable difference in the biaxial strength of IG-11 graphite was found despite the difference in the test fixture and specimen dimensions. (4) The maximum strain energy criterion was also believed to be most appropriate for PGX graphite for the first quadrant of the failure surface.

Keywords: HTGR, Nuclear Graphite, Biaxial Strength, Fracture Criteria

---

* Oak Ridge National Laboratory

高温ガス炉用黒鉛の２軸強度と破壊のクライテリア

日本原子力研究所東海研究所高温工学部
衛藤　基邦・石山新太郎・T. D. BURCHELL*
G. T. YAHR*

（1996年２月21日受理）

二種類の高温ガス炉用黒鉛について２軸応力状態における強度と破壊のクライテリアを調べた。供試材には微粒等方性のＩＧ－11黒鉛と準等方性のＰＧＸ黒鉛を用いた。電気油圧式試験機と内圧あるいはトルクを負荷する装置を組み合わせることによって，２軸応力状態を実現した。試験片は管状とし，寸法は３種類とした：(1)肉厚の影響を調べるための比較的大きな試験片（肉厚２㎜から20㎜），(2)強度データの統計的解析を行うための比較的小さな試験片（肉厚２㎜），及び(3)試験片形状及び治具の影響を調べるための，ＯＲＮＬにおいて採用されている比較的大きな試験片。

主要な結果は次の通りである。(1)データ点数が少ないため統計的な評価はできなかったが，破壊のクライテリアに及ぼす試験片肉厚の影響は顕著ではなかった。(2)比較的小さな試験片のデータを統計的に解析することによって，破壊線図の第１象限と第４象限において修正最大ひずみエネルギー説がデータ点に最もよく適合することが明らかになった。(3)ＯＲＮＬのデータは治具や試験片形状の差にもかかわらず，原研のデータのばらつきの範囲内にあった。(4)ＰＧＸ黒鉛の第１象限の破壊線図もＩＧ－11黒鉛と同様に最大ひずみエネルギー説によって表されると考えられた。

東海研究所：〒319-11　茨城県那珂郡東海村白方白根2-4
* オークリッジ国立研究所

Contents

目　　次

1.INTRODUCTION

The graphite components in the core structure of HTGR are subject to biaxial or more generally multiaxial stresses during the reactor operation. For example, prismatic fuel blocks in the reactor core are exposed to various kinds of stresses which are caused by their own weight , earthquakes, etc. as well as thermal and irradiation-induced stresses[1 - 4]. Therefore, it is necessary to provide data from which the fracture criterion under the multiaxial stress state can be derived for the design and safety evaluation of these components.

Data on the biaxial fracture criterion for the core graphite for the HTTR, High Temperature Engineering Test Reactor, were first obtained using rather large tubular specimens with different values of wall thickness. The experiment was carried out to obtain data for the derivation of fracture criterion as well as for the evaluation of the effect of specimen thickness or stress gradient on the biaxial fracture strength. The data obtained from the latter point of view were evaluated to determine appropriate dimensions of a specimen which is to be small enough to be able to machine many specimens from a graphite block for the statistical analysis on the one hand, and which is to be large enough to obtain the reliable data on the other.

The fracture criterion for the design of the graphite components in the HTTR, which has been under construction and supposed to attain criticality at the end of 1997, was set on the basis of the experimental data which had been obtained in the past, i.e., mainly the data on the larger specimens with no statistical analysis. As a result, the maximum principal stress theory and the modified Coulomb-Mohr theory were employed in the first and fourth quadrants of the failure surface, respectively [4, 5]. However, when the criterion for the HTTR was determined, the number of the data points had not been enough to make a statistical evaluation of the biaxial fracture strength of HTTR graphites.

Since then there have been extensive efforts at JAERI regarding the research on the fracture criterion of the graphites under biaxial stress state so that the adequacy of the design criteria for the HTTR graphite components can be confirmed.

In the meanwhile the biaxial fracture test of the graphite for the HTTR core components has been also carried out at Oak Ridge National Laboratory in order to examine if different fixtures and experimental techniques produce any discrepancy between the results obtained at JAERI and those at ORNL. The work has been done within the framework of JAERI/USDOE HTGR Collaboration Agreement, Annex 3: Graphite Materials Development Testing.

The purpose of this report is described as follows: (1) to summarize the biaxial fracture strength data on the larger specimens of the HTTR core graphite, IG-11, which gave a basis for the design criterion as well as the information about the effect of specimen thickness on the biaxial strength of the graphite, (2) to analyze statistically the biaxial strength of the graphite for the evaluation of the adequacy of criterion employed for the design of the HTTR core components, and (3) to cast light on the problem of the universality of the data obtained at different laboratories, i.e., JAERI and ORNL.

2. EXPERIMENTAL

Material used in the present study was IG-11 graphite which is used in the HTTR for the fuel and replaceable reflector blocks, fuel sleeve, and core support post. The tests were all done at room temperature on tubular specimens with different dimensions. Longitudinal stress, either tensile or compressive, was applied to the specimens using a servo-hydrauric test machine, while the circumferential stress, either hoop or torque, was generated by applying internal pressure or torque force to them.

2.1 Biaxial Strength Test on the Larger Specimens

Four types of specimens were used in this experiment. Figures 1(a) to (d) show the dimensions of these specimens. Cutting plan for the graphite block is shown in Fig. 2. The longitudinal axis of the block was parallel to that of the specimens. An example of the lower part of a specimen and the fixtures for the application of internal pressure to the specimen are schematically shown in Fig. 3. To prevent the oil from penetrating into it, the internal surface of the specimen was coated with rubber. Figure 4 shows the dimensions of specimen with wall thickness of 2 mm. To apply internal pressure to the specimens an apparatus the maximum oil pressure of which was around 100 MPa was annexed to a conventional servohydraulic test machine. A schematic for the testing machine is shown in Fig. 5.

2.2 Biaxial Strength Test on the Smaller Specimens

Figure 6 shows the dimensions of the smaller specimen the longitudinal axis of which was parallel to that of a graphite block. Dimensions of graphite blocks used in the test were 300 x 540 x 850 mm and 1140 mm in diameter and 750 mm in length for IG-11 and PGX graphites, respectively. The inner diameter of the PGX graphite tubular specimens was 10 mm so that their wall thickness was 5 mm.

The purpose of this report is described as follows: (1) to summarize the biaxial fracture strength data on the larger specimens of the HTTR core graphite, IG-11, which gave a basis for the design criterion as well as the information about the effect of specimen thickness on the biaxial strength of the graphite, (2) to analyze statistically the biaxial strength of the graphite for the evaluation of the adequacy of criterion employed for the design of the HTTR core components, and (3) to cast light on the problem of the universality of the data obtained at different laboratories, i.e., JAERI and ORNL.

2. EXPERIMENTAL

Material used in the present study was IG-11 graphite which is used in the HTTR for the fuel and replaceable reflector blocks, fuel sleeve, and core support post. The tests were all done at room temperature on tubular specimens with different dimensions. Longitudinal stress, either tensile or compressive, was applied to the specimens using a servo-hydrauric test machine, while the circumferential stress, either hoop or torque, was generated by applying internal pressure or torque force to them.

2.1 Biaxial Strength Test on the Larger Specimens

Four types of specimens were used in this experiment. Figures 1(a) to (d) show the dimensions of these specimens. Cutting plan for the graphite block is shown in Fig. 2. The longitudinal axis of the block was parallel to that of the specimens. An example of the lower part of a specimen and the fixtures for the application of internal pressure to the specimen are schematically shown in Fig. 3. To prevent the oil from penetrating into it, the internal surface of the specimen was coated with rubber. Figure 4 shows the dimensions of specimen with wall thickness of 2 mm. To apply internal pressure to the specimens an apparatus the maximum oil pressure of which was around 100 MPa was annexed to a conventional servohydraulic test machine. A schematic for the testing machine is shown in Fig. 5.

2.2 Biaxial Strength Test on the Smaller Specimens

Figure 6 shows the dimensions of the smaller specimen the longitudinal axis of which was parallel to that of a graphite block. Dimensions of graphite blocks used in the test were 300 x 540 x 850 mm and 1140 mm in diameter and 750 mm in length for IG-11 and PGX graphites, respectively. The inner diameter of the PGX graphite tubular specimens was 10 mm so that their wall thickness was 5 mm.

For the first quadrant of the biaxial failure surface, i.e., tension-tension, the longitudinal tensile load and internal pressure were applied to a specimen. For the fourth quadrant the load by torsion instead of internal pressure as well as the axial compressive load was applied to a specimen. A schematic for the testing machine is shown in Fig. 7.

2.3 Biaxial Strength Test Performed at ORNL

Dimensions of tubular specimens and the rig used at ORNL are shown in Fig. 8. The cutting plan for a block from which the specimens were machined is shown in Fig. 9. The longitudinal axis of the specimens was parallel to that of the block. A rigid load train facility was used for applying an axial tensile or compressive load to an internally pressurized thin-walled cylinder. Hydraulic expansion grips assured accurate alignment of the specimen. Internal pressurization of the specimen up to 6.9 MPa could be applied using water as the pressurizing medium.

3. RESULTS AND DISCUSSION

3.1 Results on the Larger Specimens

Some of the specimens with wall thickness of 15 mm or 20 mm fractured at their shoulders when an internal pressure was applied in addition to relatively large axial tensile stresses. In consideration of the fact such data will be regarded only as those for supplementary use in the following analysis.

3.1.1 Uniaxial tensile loading tests

Figures 10(a) to (d) show some results of measurements of the lateral or axial strains at the inner or outer surface of the specimens with wall thickness of 5, 10, 15 and 20 mm under the axial loading, respectively. There was no significant difference in the axial strain between the inner and outer surfaces nor was there the difference between specimens with different values of wall thickness. The ratio of the lateral strain to the axial one is almost equal to Poisson's ratio of the material measured elsewhere[6] .

These facts indicate that the strain gages were glued to a specimen properly and that no appreciable misalignment along the longitudianl axis was caused during the test.

3.1.2 Internal pressure tests

The changes in the lateral strain are shown in Fig. 11(a) and (b) as a function of internal pressure for a specimen with 5 mm wall thickness and for one with 10 mm wall thickness, respectively. Here, the axial stress at fracture was 2.5 MPa for

For the first quadrant of the biaxial failure surface, i.e., tension-tension, the longitudinal tensile load and internal pressure were applied to a specimen. For the fourth quadrant the load by torsion instead of internal pressure as well as the axial compressive load was applied to a specimen. A schematic for the testing machine is shown in Fig. 7.

2.3 Biaxial Strength Test Performed at ORNL

Dimensions of tubular specimens and the rig used at ORNL are shown in Fig. 8. The cutting plan for a block from which the specimens were machined is shown in Fig. 9. The longitudinal axis of the specimens was parallel to that of the block. A rigid load train facility was used for applying an axial tensile or compressive load to an internally pressurized thin-walled cylinder. Hydraulic expansion grips assured accurate alignment of the specimen. Internal pressurization of the specimen up to 6.9 MPa could be applied using water as the pressurizing medium.

3. RESULTS AND DISCUSSION

3.1 Results on the Larger Specimens

Some of the specimens with wall thickness of 15 mm or 20 mm fractured at their shoulders when an internal pressure was applied in addition to relatively large axial tensile stresses. In consideration of the fact such data will be regarded only as those for supplementary use in the following analysis.

3.1.1 Uniaxial tensile loading tests

Figures 10(a) to (d) show some results of measurements of the lateral or axial strains at the inner or outer surface of the specimens with wall thickness of 5, 10, 15 and 20 mm under the axial loading, respectively. There was no significant difference in the axial strain between the inner and outer surfaces nor was there the difference between specimens with different values of wall thickness. The ratio of the lateral strain to the axial one is almost equal to Poisson's ratio of the material measured elsewhere[6] .

These facts indicate that the strain gages were glued to a specimen properly and that no appreciable misalignment along the longitudianl axis was caused during the test.

3.1.2 Internal pressure tests

The changes in the lateral strain are shown in Fig. 11(a) and (b) as a function of internal pressure for a specimen with 5 mm wall thickness and for one with 10 mm wall thickness, respectively. Here, the axial stress at fracture was 2.5 MPa for

the latter case and 5.1 MPa for the former. In both cases the lateral inner strain at fracture seems to be nearly equal to the fracture strain measured during the uniaxial tensile test. As is expected, the difference between the inner and the outer strains is larger, the thicker, the wall. The lateral fracture strain is shown in Figs. 12(a) and (b) as a function of axial stress. Here, one can see that the lateral fracture strain decreases in the axial stress increases, which is believed to correspond to the fact that in the first quadrant of the biaxial failure surface the significant strength decrease is observed at an angle of around 45 degrees, i.e., the ratio of hoop stress to tensile axial stress, $\sigma_H / \sigma_T = 1$.

3.1.3 Failure surface

Figure 13 summarizes the biaxial strength data on specimens with different wall thicknesses. In this figure the fracture criterion for the design of the graphite components of the HTTR are also shown as a solid line. Almost all the data points are at the outside of the area designated by the line. However, the safety margin is not indicated quantitatively in the figure. For this reason the statistical approach to the data on the smaller specimens will be done in the next experiment.

Effect of wall thickness is not significant in the present experiment. Besides, the hoop stress of the specimens with 10 mm wall thickness is smaller than that for the thinner walled specimens at an angle of 45 degrees in the first quadrant of the failure surface. This is probably because the specimens failured at their shoulders.

It is apparent from the results shown in Fig. 14 that the hoop fracture stress increases with increasing wall thickness when the axial stress is zero. However, for the specimens subject to the higher axial stress the tendency above is not clearly seen, which suggests that the more data points be necessary to judge if such a tendency is also observed under an axial stress.

Figure 15 shows the ratio of the hoop fracture stress at the outer surface to that at the inner surface, i.e., hoop fracture stress referred to so far, and the ratio of the outer hoop fracture strain to the inner one. The strains were measured directly from the output of the strain gages. Here, when the ratio of the outer strain to the inner strain is plotted, the difference in the axial stress between the specimens was disregarded so that the specimens with the same wall thickness were treated as those which represented one group. In this figure one can see that the strain ratio seems to be smaller than the stress ratio except for the specimens with wall thickness of 15 mm for which some experimental error might be incurred.

The result may result from the fact that the stress was estimated on the basis of the elastic theory using the equation,

$$\frac{\sigma_{HO}}{\sigma_{HI}} = \frac{2}{(r_O / r_I)^2 + 1} \quad (1)$$

σ_{HO} : Outer hoop stress, σ_{HI} : Inner hoop stress,

r_O : Outer radius, r_I : Inner radius,

whereas the ratio of the strain well reflects the inelastic character of the graphite.

On the basis of the elastic theory σ_{HO}/σ_{HI} is expressed as

$$\frac{\sigma_{HO}}{\sigma_{HI}} = \frac{E e_{HO}}{E e_{HI}} \quad (2)$$

Here, E is the elastic constant and e_{HO}, e_{HI} are calculated strains at the outer and inner surfaces, respectively.

The inelasticity of polycrystalline graphite has been often approximated as [7,8]

$$\varepsilon = (1/E)\sigma + B\sigma^2 . \quad (3)$$

From eq.(3), one can deduce that

$$\varepsilon_{HI} = (1/E)\,\sigma_{HI} + B\,\sigma_{HI}^2 = \sigma_{HI}(1/E + B\sigma_{HI})$$
$$\varepsilon_{HO} = (1/E)\,\sigma_{HO} + B\,\sigma_{HO}^2 = \sigma_{HO}(1/E + B\sigma_{HO}) \quad (4)$$

From eq.(4),

$$\varepsilon_{HO} / \varepsilon_{HI} = (\sigma_{HO} / \sigma_{HI})\{(1/E + B\sigma_{HO}) /(1/E + B\sigma_{HI})\} \quad (5)$$

Since $\sigma_{HO} < \sigma_{HI}$, $(1/E + B\sigma_{HO}) /(1/E + B\sigma_{HI}) < 1$.

From the above inequality and eq.(5),

$$\varepsilon_{HO} / \varepsilon_{HI} < \sigma_{HO} / \sigma_{HI} . \quad (6)$$

This is in agreement with the tendency observed in the experimental results.

3.2 Biaxial Strength Test of the Smaller Specimens

3.2.1 The first quadrant of the failure surface for IG-11 and PGX graphites

Figs. 16 and 17 show the results of biaxial strength test in the condition of the first quadarant of the failure surface(tesnsion-tension) for IG-11 and PGX graphites, respectively. 5 to 25 specimens were tested at each level of the ratio of the hoop stress to the axial one(σ_H / σ_A) which ranged from 0 to 3.15.

As one can see in the figures, the data points show fairly large scatters for both IG-11 and PGX graphites. It is found in these figures that the axial fracture and hoop fracture stresses decrease in the biaxial stress state, especially when the ratio of the hoop to axial stresses is around 1, and that equi-biaxial strength decreases about 40 % and 20 % from the uniaxial strength for IG-11 and PGX graphites, respectively. Thus, the data shown in Figs. 16 and 17 were analyzed

statistically as is shown in Fig. 18 and 19, and Figs. 20 and 21 corresponding to Figs. 16 and 17, respectively. Here, the fracture probability of both IG-11 and PGX graphite specimens is shown as a function of the axial stress or hoop stress normalized to the mean tensile strength. Parameters are the ratio of the hoop stress to axial stress, which ranges from 0 to 8.17 for IG-11 graphite and 0 to 3.0 for PGX graphite. The lines fitted to the data points in these figures are drawn on the normal distribution function:

$$\text{Fracture probability } F = A \exp \{m (\sigma / \sigma_t)\} \quad (7)$$

Here, A and m are scale and shape factors, respectively. It is seen that the data points are well expressed by the normal distribution function.

3.2.2 The fourth quadrant of the failure surface for IG-11 graphite

Specimens of IG-11 graphite specimens were tested to obtain data for the fourth quadrant of the failure surface. To realize the biaxial stress state the axial compressive load as well as torque was applied to a specimen. Fig. 22 shows the results of the test. As was the case for the larger specimens the fracture stress decreases with increasing compressive stress or circumferential tensile stress for the range of stress ratio, $\sigma_{\text{compressive}} / \sigma_{\text{circumferential tensile}} < -1.3$.

Figures 23 and 24 show the fracture probability plotted on the normal probability paper as a function of tensile fracture stress normalized to the mean tensile strength. It is believed that the data points are well represented by the normal distribution function as was the case for the first quadrant of the failure surface.

3.2.3 Fracture criterion of the graphite

Macroscopic fracture criterion for the graphites tested in the present experiment are discussed here. There have been several theories of the fracture criterion, e.g., the maximum principal stress theory, maximum shear stress theory, naximum shear strain energy theory, etc.

Figure 25 shows all the data points obtained in the present experiment for IG-11 graphite. Figure 26 shows the same data points which are normalized to the mean tensile strength for the tensile stress axis and hoop stress axis of the first quadrant, and to the mean compressive strength for the compressive stress axis of the fourth quadrant.

In the figure the solid line and the chain line represent the modified maximum strain energy criterion and the maximum principal stress criterion, respectively. Here, the modified maximum strain energy criterion is expressed as

$$\sigma_1^2 + \sigma_2^2 = 1 \quad (8)$$

$\sigma_1 = \sigma_{\text{axial}} / \sigma_{\text{tensile or compressive}}$, $\sigma_2 = \sigma_{\text{hoop or circumferential}} / \sigma_{\text{tensile}}$.

Apparently, the maximum principal stress criterion is not fitted well to the data points. The modified maximum strain energy criterion seems to be well applicable to the data points though the theory gives a conservative criterion at around $\sigma_1/\sigma_2 = 1$, which implies that the safer design can be drawn from the theory.

It is seen in the fourth quadrant that the modified maximum strain energy theory gives the most appropriate criterion on the basis of the data points obtained here. Though the modified maximum shear strain energy and modified Mohr's theories were tried to be fitted to the data, neither of them gave the better fittness to the data points than did the modified maximum strain energy theory.

Results similar to those in Figs. 25 and 26 are shown in Figs. 27 and 28 for PGX graphite. Ho et al. [3] reported that the biaxial strength of PGX graphite can be expressed on the basis of the maximum principal stress theory. This is probably because the grain size of the specimens they tested in their experiment was about 2.5 mm whereas the same grade of graphite here in the present experiment comprised grains the maximum size of which was 0.8 mm. From these considerations, differently from the conclusions derived by Ho et al.[3] , Tzung[9] and Tang[2], PGX graphite seems to obey the modified maximum strain energy theory, though the solid line in Fig. 27 may be considered somewhat too conservative. In fact, specimens with wall thickness of 2 mm were fractured by the smaller hoop stress, as is shown in Fig. 27. The test on these specimens 2 mm in wall thickness was done only in the condition that the fracture would be caused by the hoop stress only where no axial stress was caused or axial stress only where no hoop stress was caused.

The fracture probability: The fracture criteria for the 1 % fracture probability and 95 % confidence limit are shown in Figs. 26 and 28 for IG-11 and PGX graphites, respectively. Though the design curves employed for the HTTR are conservative, it is believed that theoretically the modified maximum strain energy criterion is better fitted to the experimental data.

The difference in the shape factor between compression and tension: The data points shown in Figs. 23 and 24 were fitted to the normal distribution using an equation, $F = a + m\ normal\ function$ [stress level].

Here, F: the fracture probability, a: scale factor, m: shape factor.

Fig. 29 shows the m-value as a function of stress ratio. For the tensile fracture stress the values of m tend to increase with increasing ratio of compressive stress to tensile stress, whereas for the compressive fracture stress the m-values remain to be almost unchanged irrespective of the stress ratio. The fact indicates that the scatter of the tensile fracture stress becomes larger with decreasing stress ratio, i.e., as the compressive stress becomes comparable to the tensile stress. The cause

for this behavior is yet to be investigated.

In the case of the first quadrant of the failure surface, i.e., tension-tension, the *m*-value for the axial tensile fracture stress tended to decrease with increasing ratio of the axial or the hoop stress to the mean tensile strength. On the other hand, the value for the hoop fracture stress seemed to become larger as the ratio of the hoop stress to the mean tensile strength increased.

3.2.4 Comparison between the ORNL and JAERI data

The data points obtained at ORNL are plotted in Fig. 30 together with those of JAERI. Probably because the specimen size, particularly the wall thickness was the larger for ORNL than for JAERI, the scatter of the data is much smaller for the former case. However, the ORNL data fall within the scatter band of the JAERI data. The fact suggests that the above discussion on the JAERI data is also made on the ORNL data.

One difference between ORNL and JAERI data was that at ORNL the axial tensile fracture stress was about 15 % larger than the hoop fracture stress. This difference may result from the difference in the fixtures between the two facilities.

4. CONCLUSIONS

The fracture criteria at the biaxial stress state were examined for a fine-grained isotropic nuclear graphite, IG-11 and a medium size-grained semi-isotropic nuclear graphite, PGX. To realize the biaxial stress state the axial loading, either tensile or compressive, and the internal pressure or torque were applied to several types of tubular specimens. From the aspect of their size, the specimens were classified into three categories: (1) the larger ones with different wall thicknesses which were tested for the purpose of investigating the effect of wall thickness on the biaxial strength, (2) the smaller ones which were tested for the purpose of obtaining data for the statistical analysis, and (3) specimens tested at ORNL which were tested to examine if there is any difference in the strength data depending on the rig and specimen dimensions.

Main Conclusions are:

1) As for the failure surface, no significant difference was observed between the IG-11 graphite specimens with thick wall(20 mm) and with thin wall(2 mm) though the number of specimens tested was not large enough to evaluate the data statistically.
2) The ratio of the lateral fracture strain at the outer surface to that at the inner surface decreased with increasing wall thickness. This ratio was smaller than

for this behavior is yet to be investigated.

In the case of the first quadrant of the failure surface, i.e., tension-tension, the *m*-value for the axial tensile fracture stress tended to decrease with increasing ratio of the axial or the hoop stress to the mean tensile strength. On the other hand, the value for the hoop fracture stress seemed to become larger as the ratio of the hoop stress to the mean tensile strength increased.

3.2.4 Comparison between the ORNL and JAERI data

The data points obtained at ORNL are plotted in Fig. 30 together with those of JAERI. Probably because the specimen size, particularly the wall thickness was the larger for ORNL than for JAERI, the scatter of the data is much smaller for the former case. However, the ORNL data fall within the scatter band of the JAERI data. The fact suggests that the above discussion on the JAERI data is also made on the ORNL data.

One difference between ORNL and JAERI data was that at ORNL the axial tensile fracture stress was about 15 % larger than the hoop fracture stress. This difference may result from the difference in the fixtures between the two facilities.

4. CONCLUSIONS

The fracture criteria at the biaxial stress state were examined for a fine-grained isotropic nuclear graphite, IG-11 and a medium size-grained semi-isotropic nuclear graphite, PGX. To realize the biaxial stress state the axial loading, either tensile or compressive, and the internal pressure or torque were applied to several types of tubular specimens. From the aspect of their size, the specimens were classified into three categories: (1) the larger ones with different wall thicknesses which were tested for the purpose of investigating the effect of wall thickness on the biaxial strength, (2) the smaller ones which were tested for the purpose of obtaining data for the statistical analysis, and (3) specimens tested at ORNL which were tested to examine if there is any difference in the strength data depending on the rig and specimen dimensions.

Main Conclusions are:

1) As for the failure surface, no significant difference was observed between the IG-11 graphite specimens with thick wall(20 mm) and with thin wall(2 mm) though the number of specimens tested was not large enough to evaluate the data statistically.
2) The ratio of the lateral fracture strain at the outer surface to that at the inner surface decreased with increasing wall thickness. This ratio was smaller than

that of the outer fracture hoop stress to the inner one which were calculated on the basis of the elastic theory.

3) The fracture hoop stress increased with increasng wall thickness when no axial load was applied to a specimen. However, no increase in the fracture hoop stress was detected under the axial load.
4) On the basis of the statistical analysis of the data on the smaller specimens, the modified maximum strain energy criterion gave the best fit to the data points both in the first and in the fourth quadrants of the failure surface.
5) The data points obtained at ORNL fell on the scatter band of the JAERI data, which indicated that no appreciable difference in the biaxial strength of IG-11 graphite was found despite the differences in the test fixture and specimen dimensions.
6) The maximum strain energy criterion was also believed to be most appropriate for PGX graphite though one had to take the effect of grain size into account.

Acknowledgements: The data obtained at JAERI have been accumulated thanks to extensive efforts made by a number of people such as Messrs. T. Arai, Y. Nishiyama, and M. Matsumoto. The authors are heartily grateful to them. They also thank Mr.Y. Muto for a lot of valuable comments and discussion.

REFERENCES

1. R.E. Ely, J. Am. Cer. Soc. 48(1965)505.
2. P.Y. Yang, GA-A15333(1979).
3. F.H. Ho, Proc. of SMiRT 7, Chicago, USA, L4/6, 127(1983).
4. S. Saito et al., JAERI-1332(1994).
5. T. Iyoku et al., Nucl. Eng. & Design 132(1991)23.
6. T. Arai et al., JAERI-M 92-085.
7. G.M. Jenkins, Britt. J. Appl. Phys. 13(1962)30.
8. M. Eto and T. Oku, J. Nucl. Mater. 57(1975)198.
9. F-K. Tzung, GA-A15573(1979).

that of the outer fracture hoop stress to the inner one which were calculated on the basis of the elastic theory.

3) The fracture hoop stress increased with increasng wall thickness when no axial load was applied to a specimen. However, no increase in the fracture hoop stress was detected under the axial load.
4) On the basis of the statistical analysis of the data on the smaller specimens, the modified maximum strain energy criterion gave the best fit to the data points both in the first and in the fourth quadrants of the failure surface.
5) The data points obtained at ORNL fell on the scatter band of the JAERI data, which indicated that no appreciable difference in the biaxial strength of IG-11 graphite was found despite the differences in the test fixture and specimen dimensions.
6) The maximum strain energy criterion was also believed to be most appropriate for PGX graphite though one had to take the effect of grain size into account.

Acknowledgements: The data obtained at JAERI have been accumulated thanks to extensive efforts made by a number of people such as Messrs. T. Arai, Y. Nishiyama, and M. Matsumoto. The authors are heartily grateful to them. They also thank Mr.Y. Muto for a lot of valuable comments and discussion.

REFERENCES

1. R.E. Ely, J. Am. Cer. Soc. 48(1965)505.
2. P.Y. Yang, GA-A15333(1979).
3. F.H. Ho, Proc. of SMiRT 7, Chicago, USA, L4/6, 127(1983).
4. S. Saito et al., JAERI-1332(1994).
5. T. Iyoku et al., Nucl. Eng. & Design 132(1991)23.
6. T. Arai et al., JAERI-M 92-085.
7. G.M. Jenkins, Britt. J. Appl. Phys. 13(1962)30.
8. M. Eto and T. Oku, J. Nucl. Mater. 57(1975)198.
9. F-K. Tzung, GA-A15573(1979).

that of the outer fracture hoop stress to the inner one which were calculated on the basis of the elastic theory.

3) The fracture hoop stress increased with increasng wall thickness when no axial load was applied to a specimen. However, no increase in the fracture hoop stress was detected under the axial load.
4) On the basis of the statistical analysis of the data on the smaller specimens, the modified maximum strain energy criterion gave the best fit to the data points both in the first and in the fourth quadrants of the failure surface.
5) The data points obtained at ORNL fell on the scatter band of the JAERI data, which indicated that no appreciable difference in the biaxial strength of IG-11 graphite was found despite the differences in the test fixture and specimen dimensions.
6) The maximum strain energy criterion was also believed to be most appropriate for PGX graphite though one had to take the effect of grain size into account.

Acknowledgements: The data obtained at JAERI have been accumulated thanks to extensive efforts made by a number of people such as Messrs. T. Arai, Y. Nishiyama, and M. Matsumoto. The authors are heartily grateful to them. They also thank Mr.Y. Muto for a lot of valuable comments and discussion.

REFERENCES

1. R.E. Ely, J. Am. Cer. Soc. 48(1965)505.
2. P.Y. Yang, GA-A15333(1979).
3. F.H. Ho, Proc. of SMiRT 7, Chicago, USA, L4/6, 127(1983).
4. S. Saito et al., JAERI-1332(1994).
5. T. Iyoku et al., Nucl. Eng. & Design 132(1991)23.
6. T. Arai et al., JAERI-M 92-085.
7. G.M. Jenkins, Britt. J. Appl. Phys. 13(1962)30.
8. M. Eto and T. Oku, J. Nucl. Mater. 57(1975)198.
9. F-K. Tzung, GA-A15573(1979).

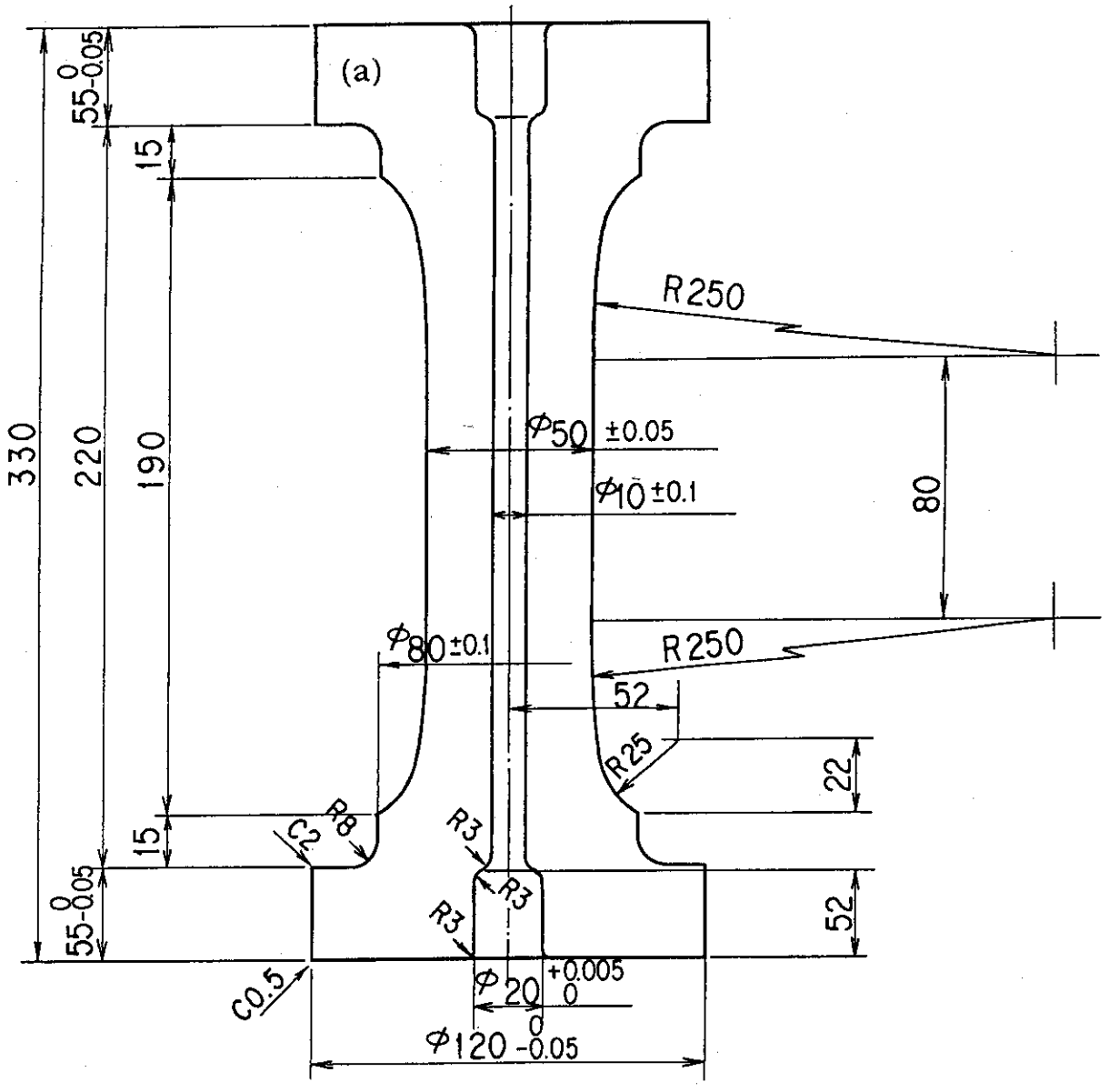

Fig. 1 Dimensions of the larger specimens with wall thickness of (a) 20 mm, (b) 15 mm, (C) 10 mm and (d) 5 mm.

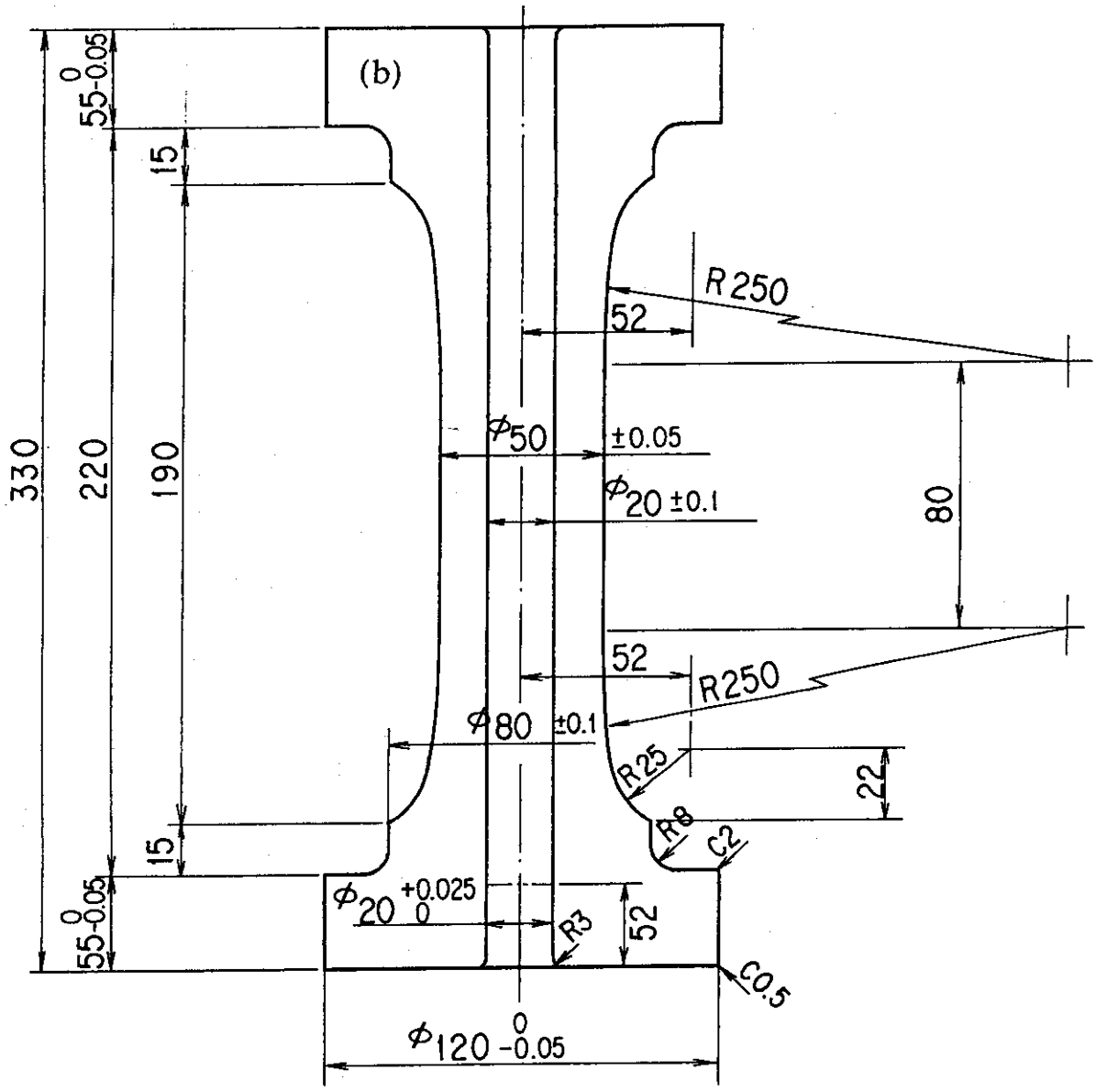

Fig. 1 Dimensions of the larger specimens with wall thickness of (a) 20 mm, (b) 15 mm, (C) 10 mm and (d) 5 mm.

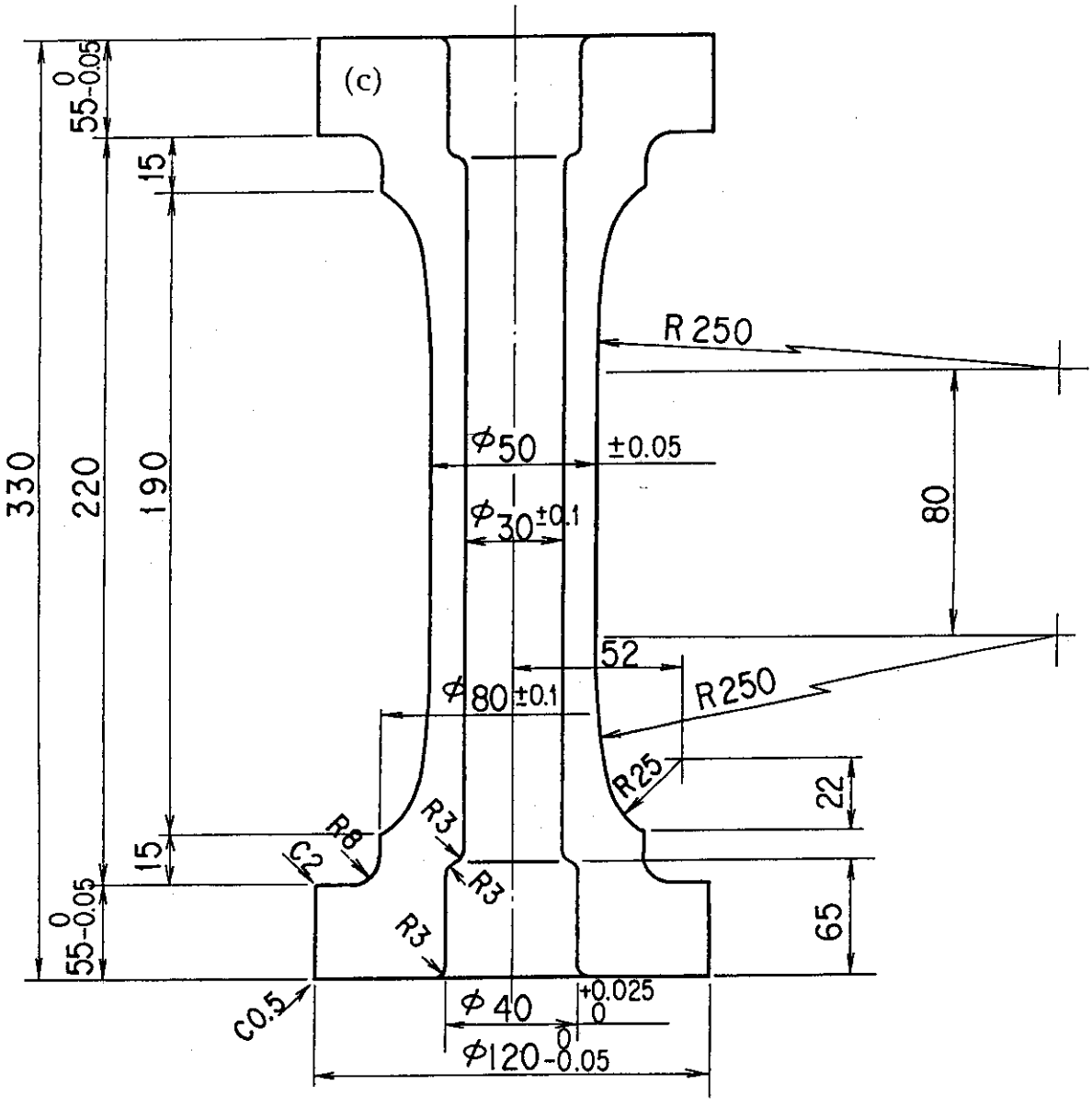

Fig. 1 Dimensions of the larger specimens with wall thickness of (a) 20 mm, (b) 15 mm, (C) 10 mm and (d) 5 mm.

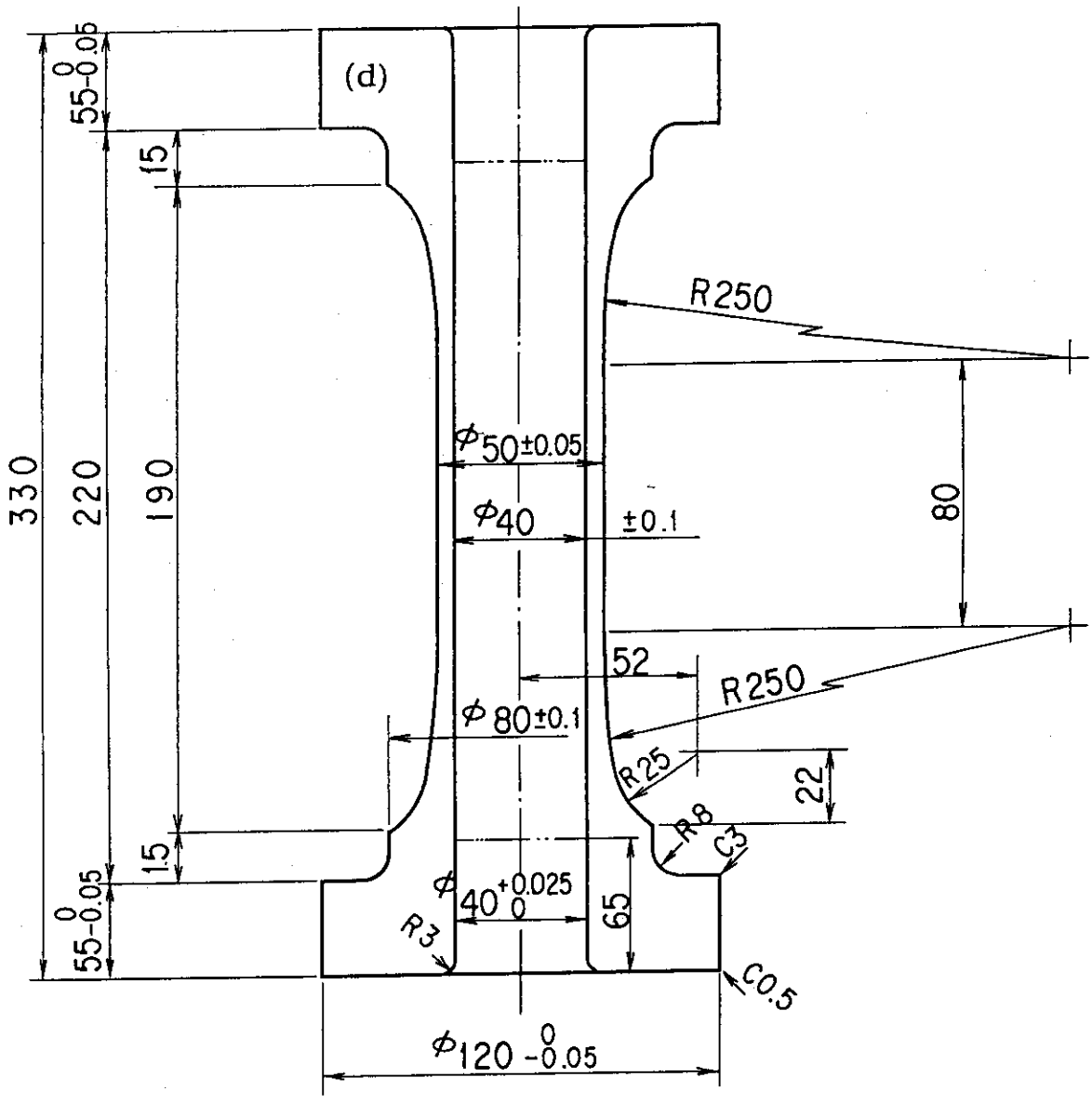

Fig. 1 Dimensions of the larger specimens with wall thickness of (a) 20 mm, (b) 15 mm, (C) 10 mm and (d) 5 mm.

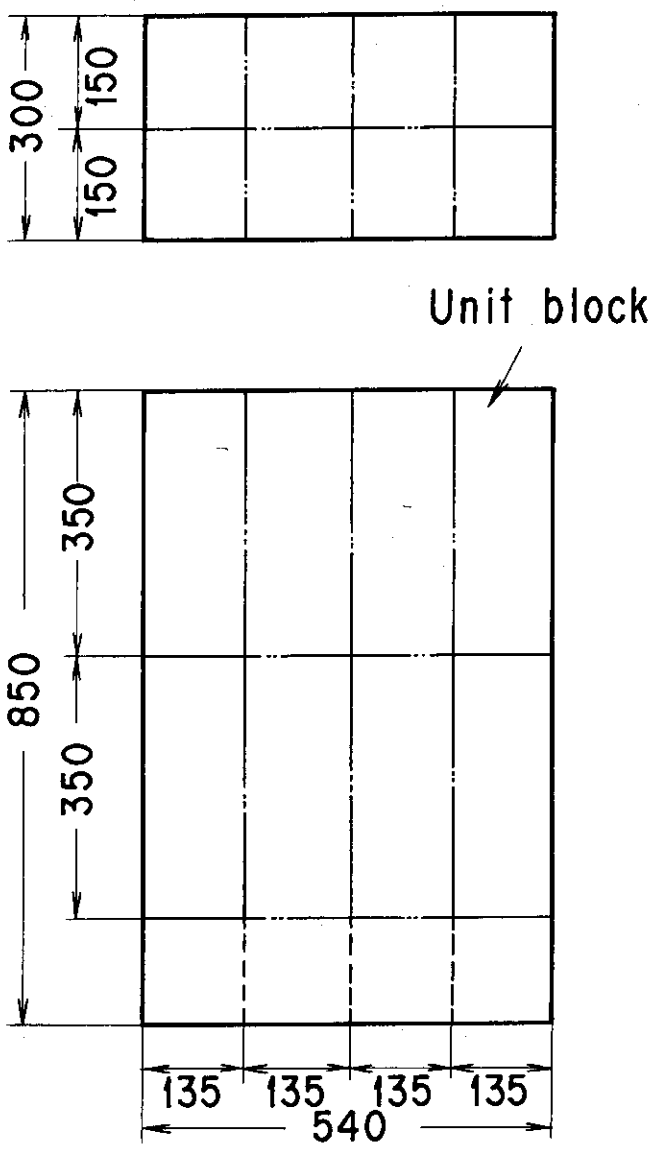

Fig. 2 Cutting plan for an IG-11 graphite block.

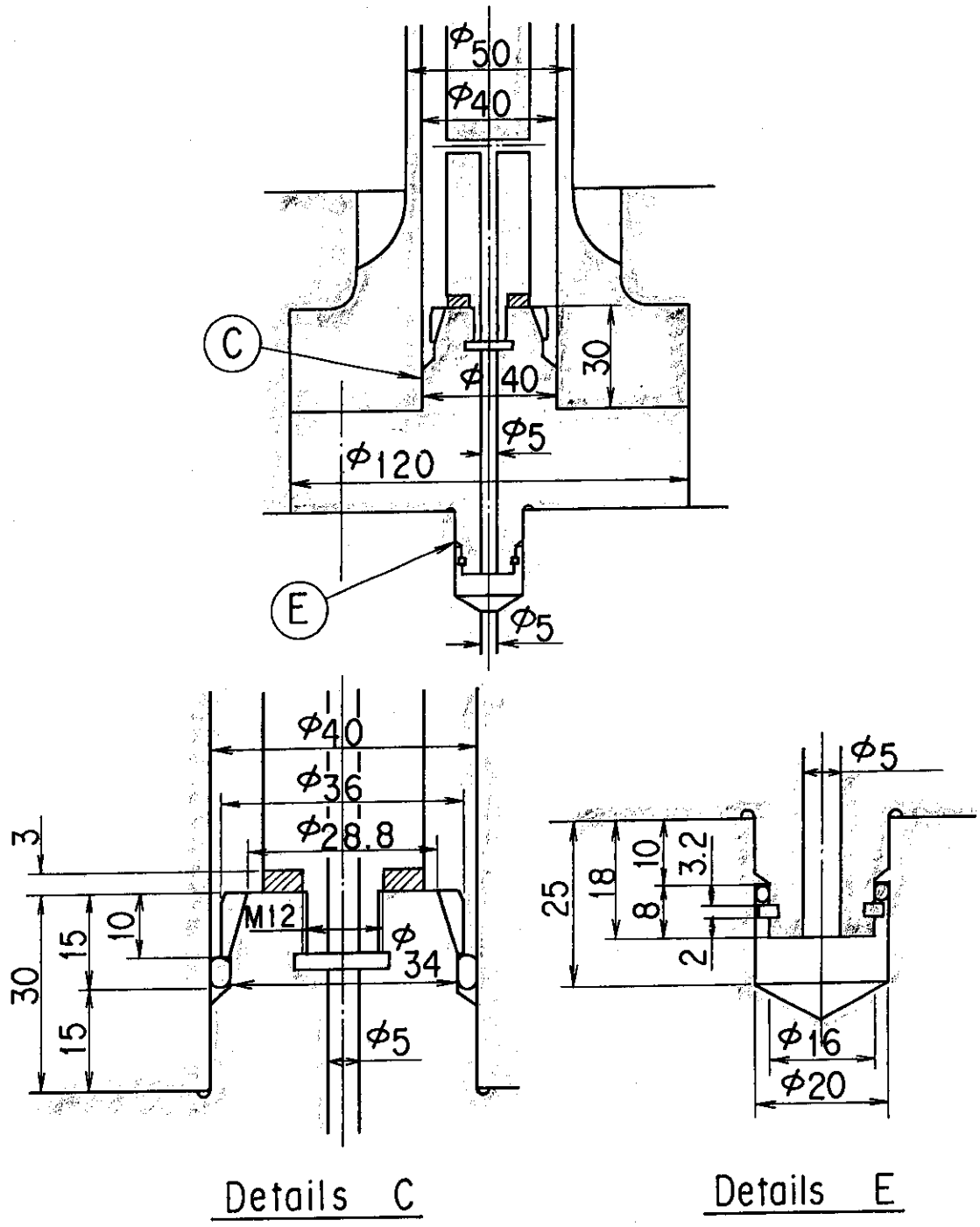

Fig. 3 The details of the lower part of a specimen and the jig for the application of internal pressure.

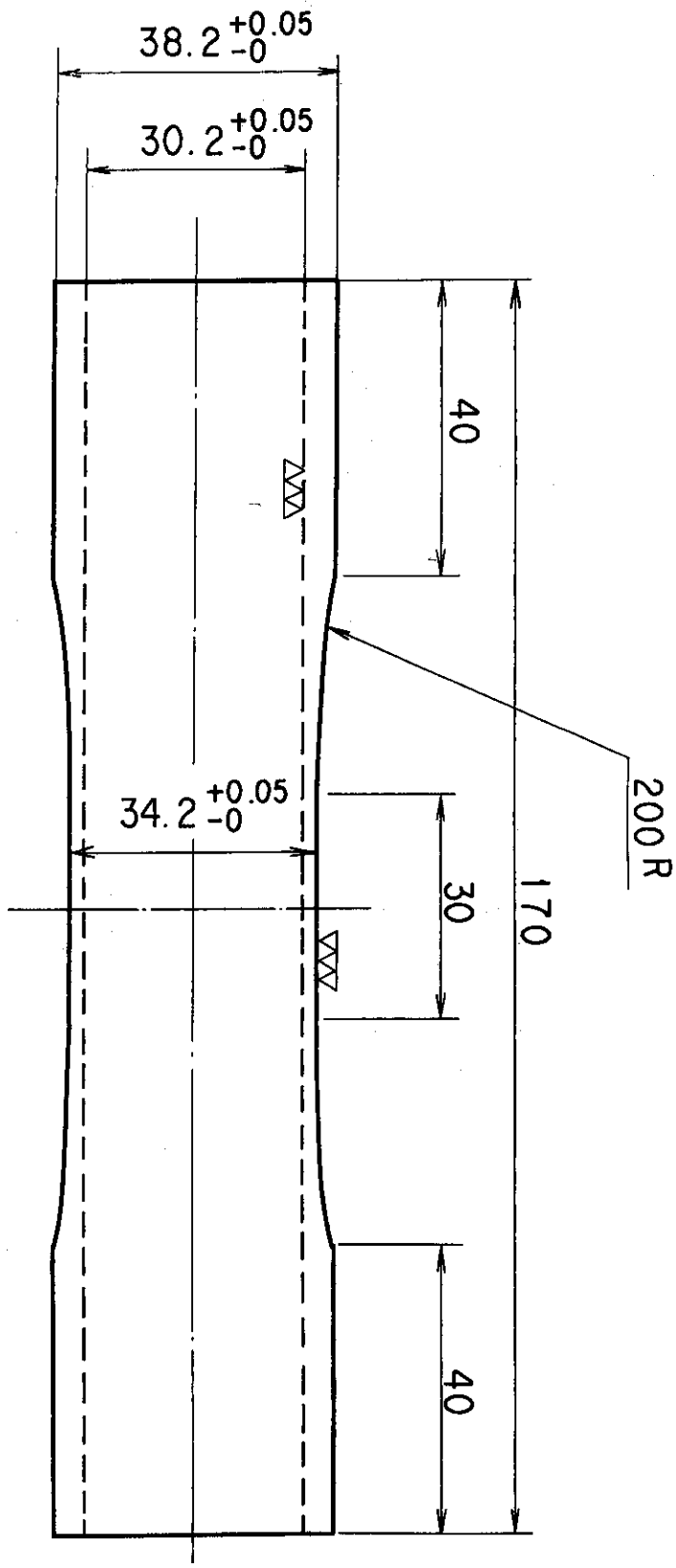

Fig. 4 Dimensions of the specimen with wall thickness of 2 mm.

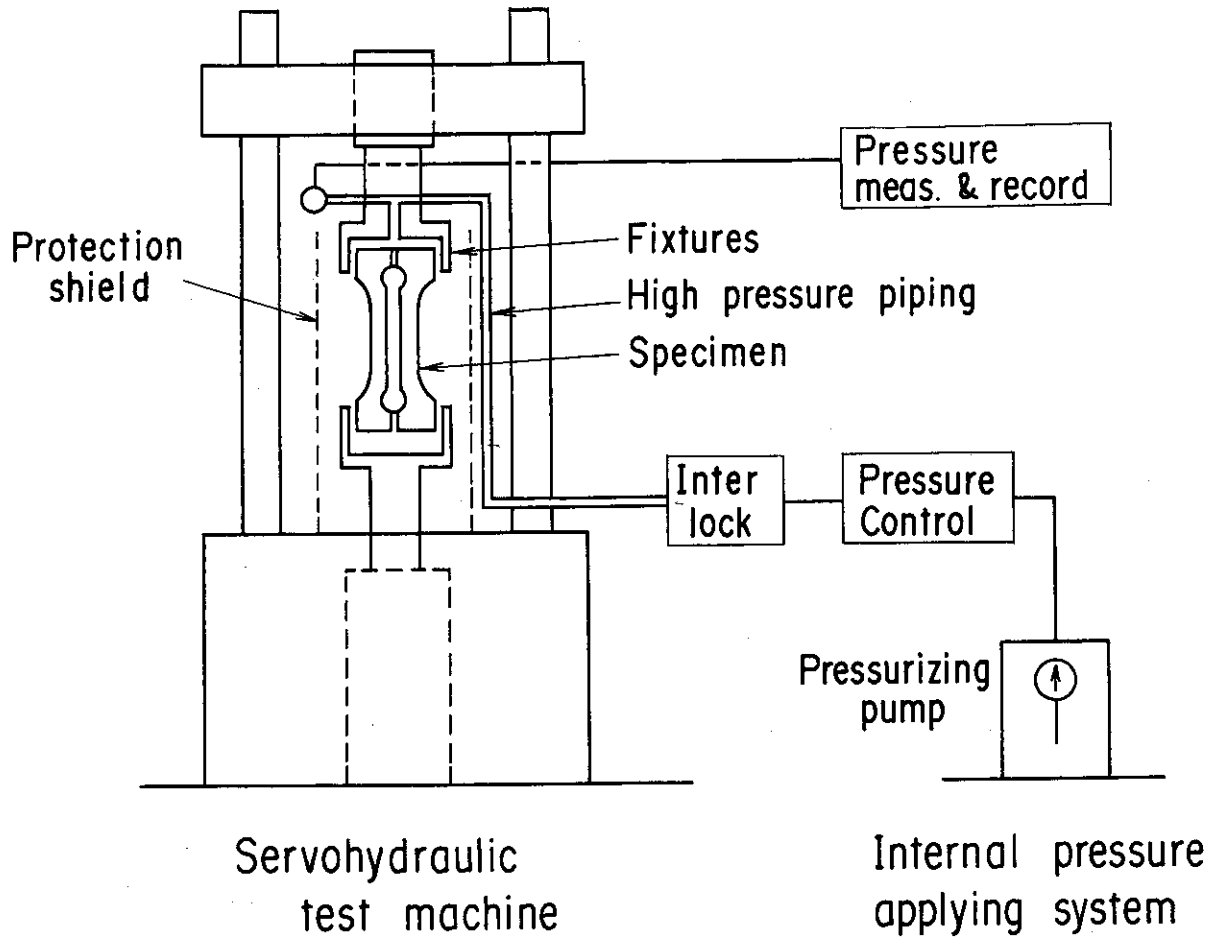

Fig. 5 A schematic for test on the smaller specimen.

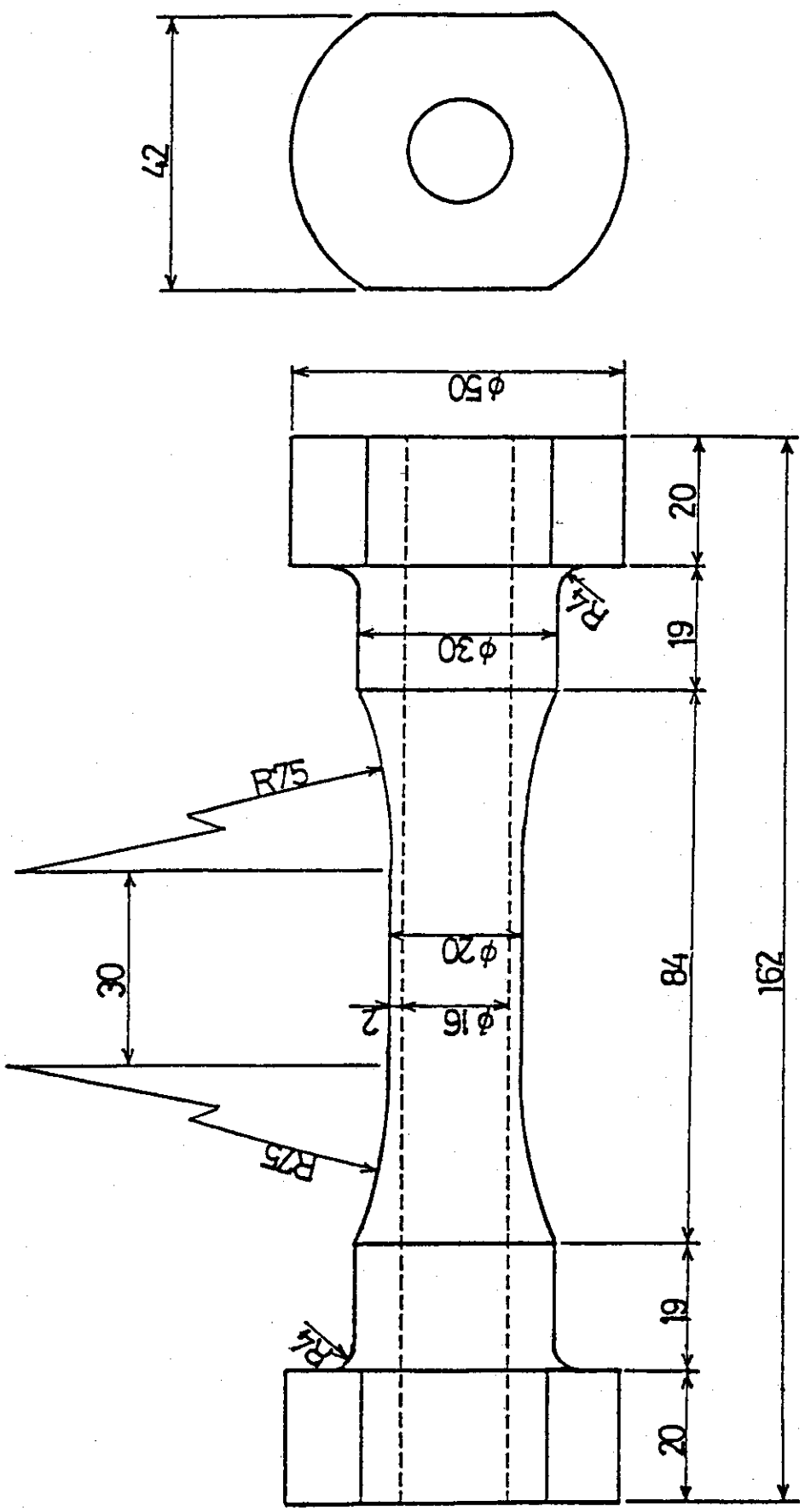

Fig. 6 Dimensions of the smaller specimens.

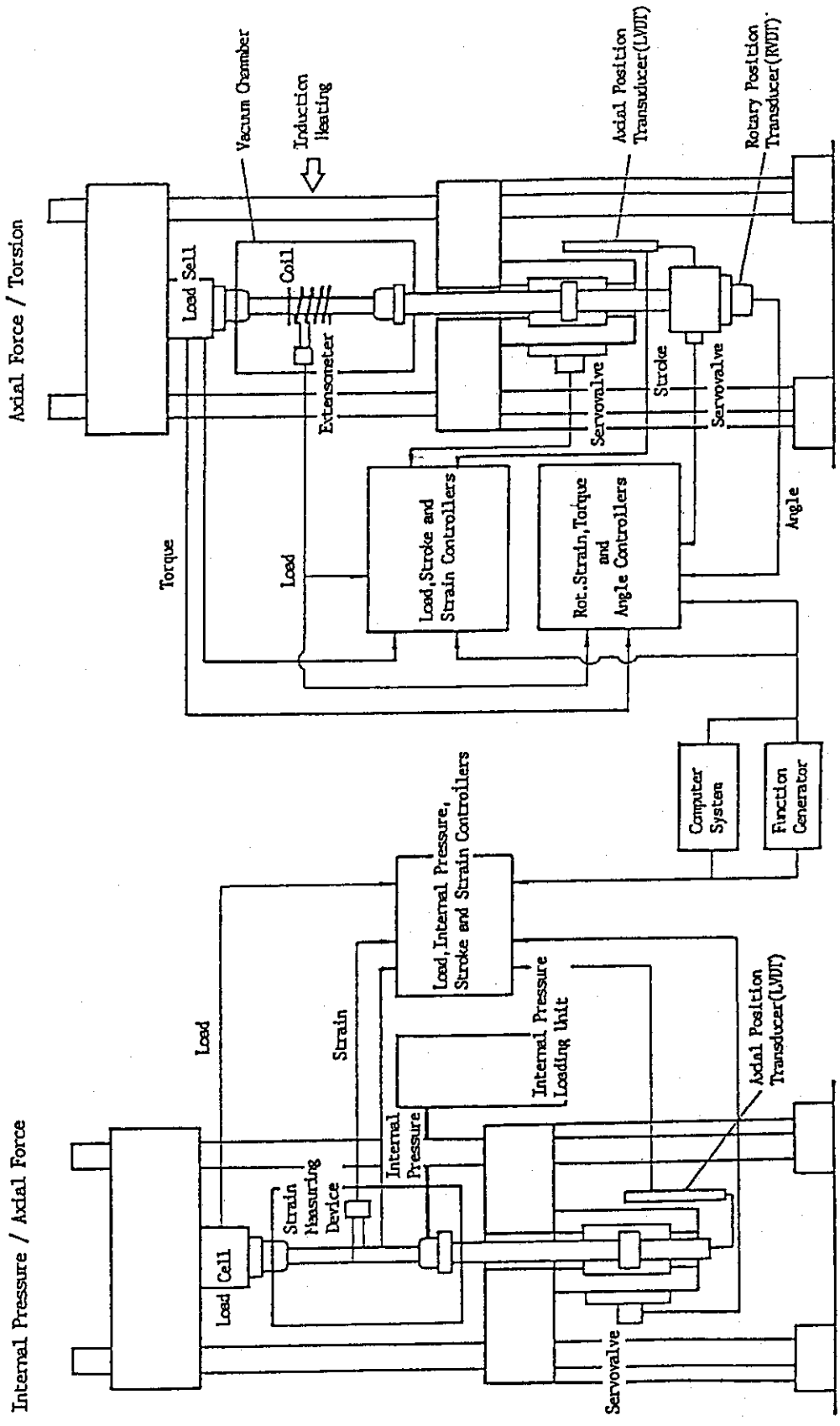

Fig. 7 A schematic illustration for the biaxial fracture strength testing machine.

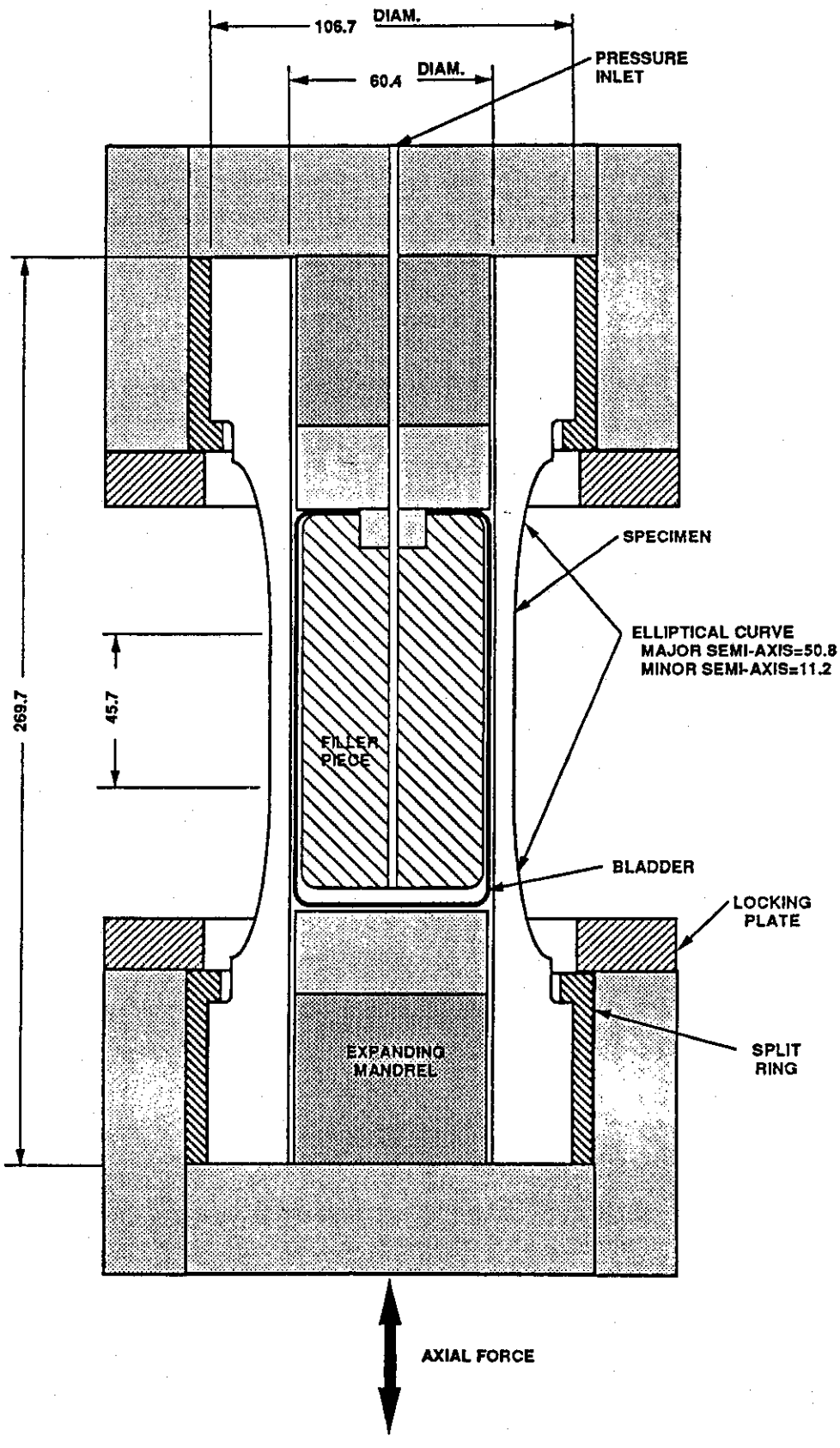

Fig. 8 Biaxial loading arrangement and test rig.

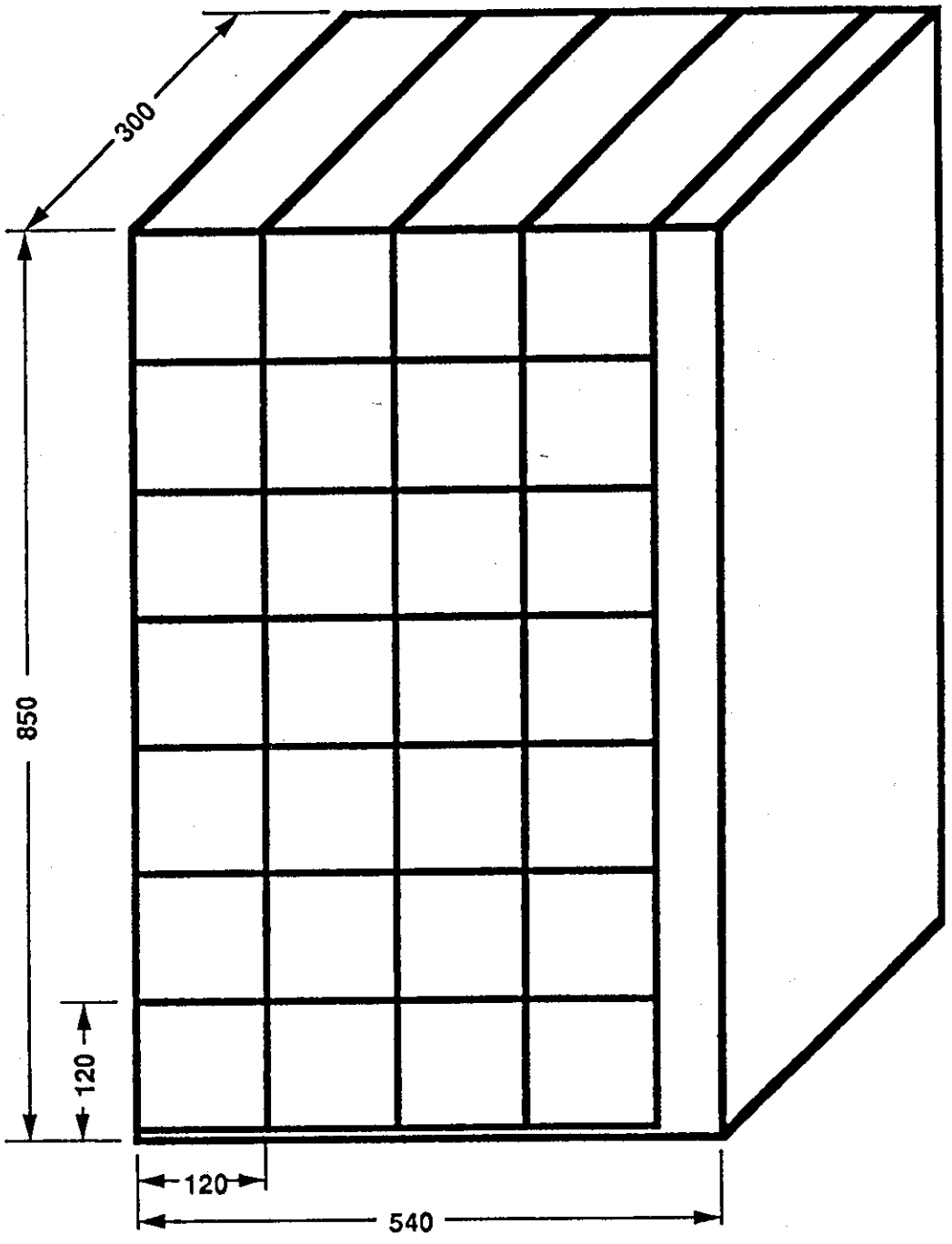

Fig. 9 Cutting plan for the blocks from which specimens were machined.

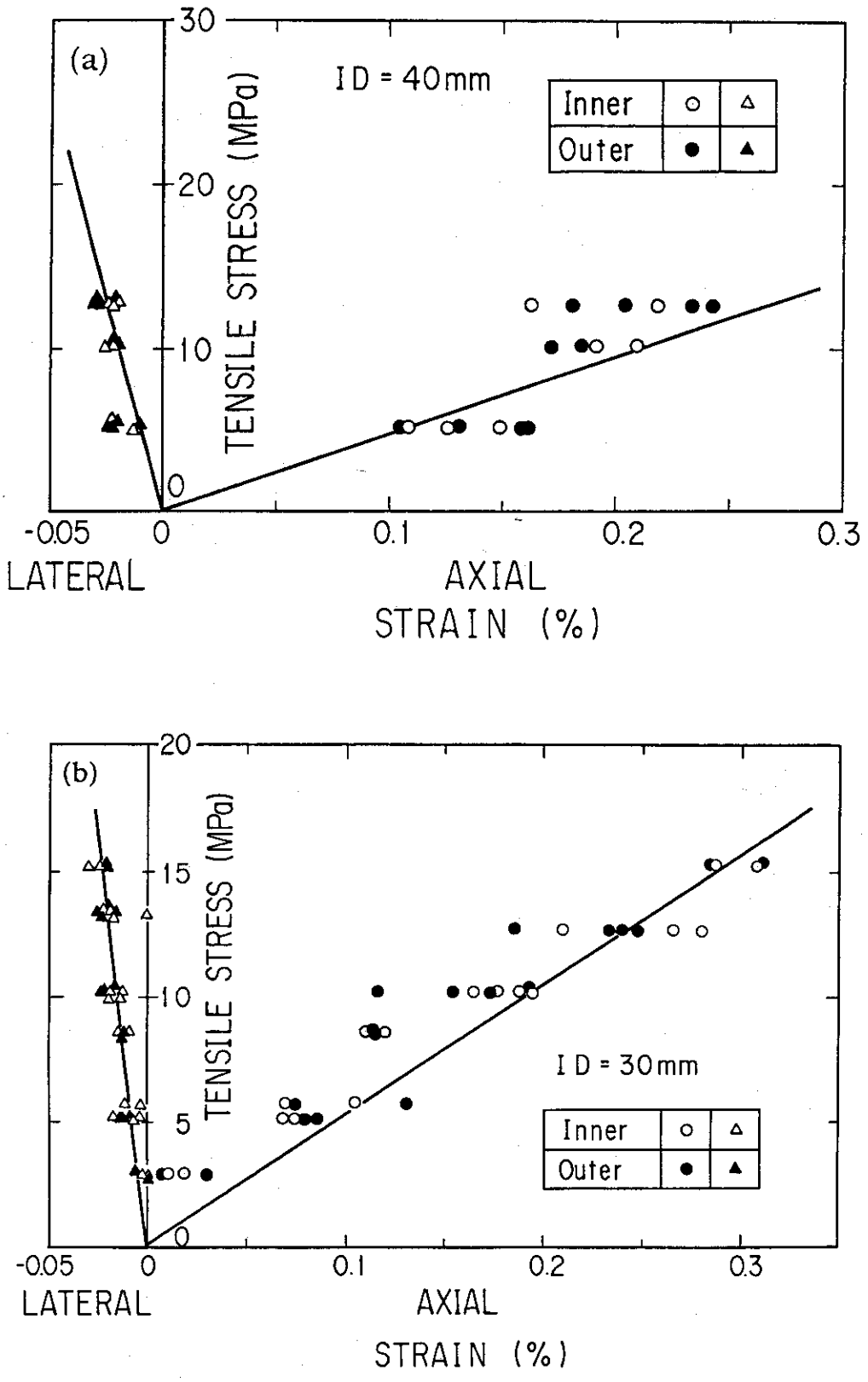

Fig.10 Axial or lateral strain as a function of axial tensile stress for specimens with wall of (a) 5 mm, (b) 10 mm, (c) 15 mm and (d) 20 mm.

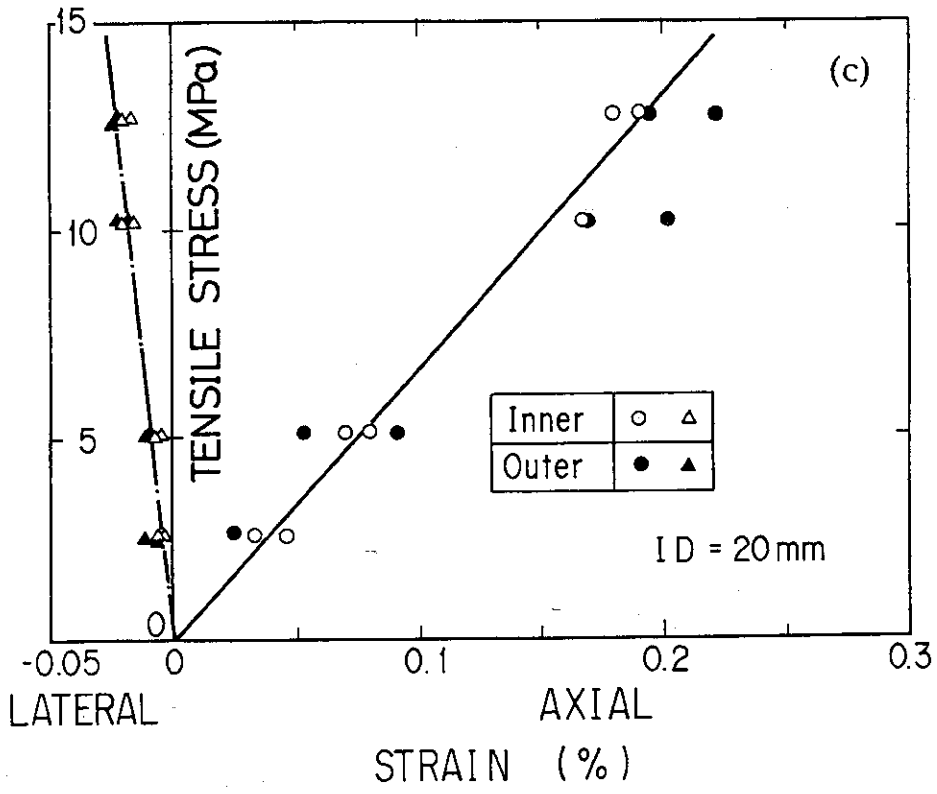

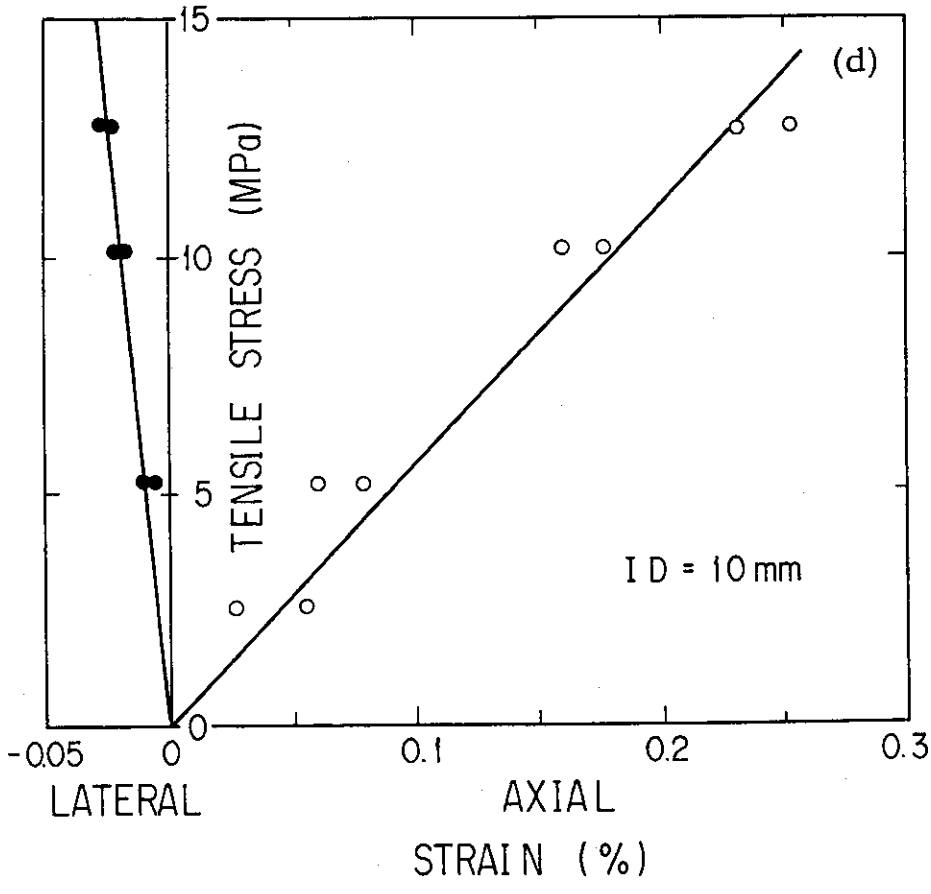

Fig.10 Axial or lateral strain as a function of axial tensile stress for specimens with wall of (a) 5 mm, (b) 10 mm, (c) 15 mm and (d) 20 mm.

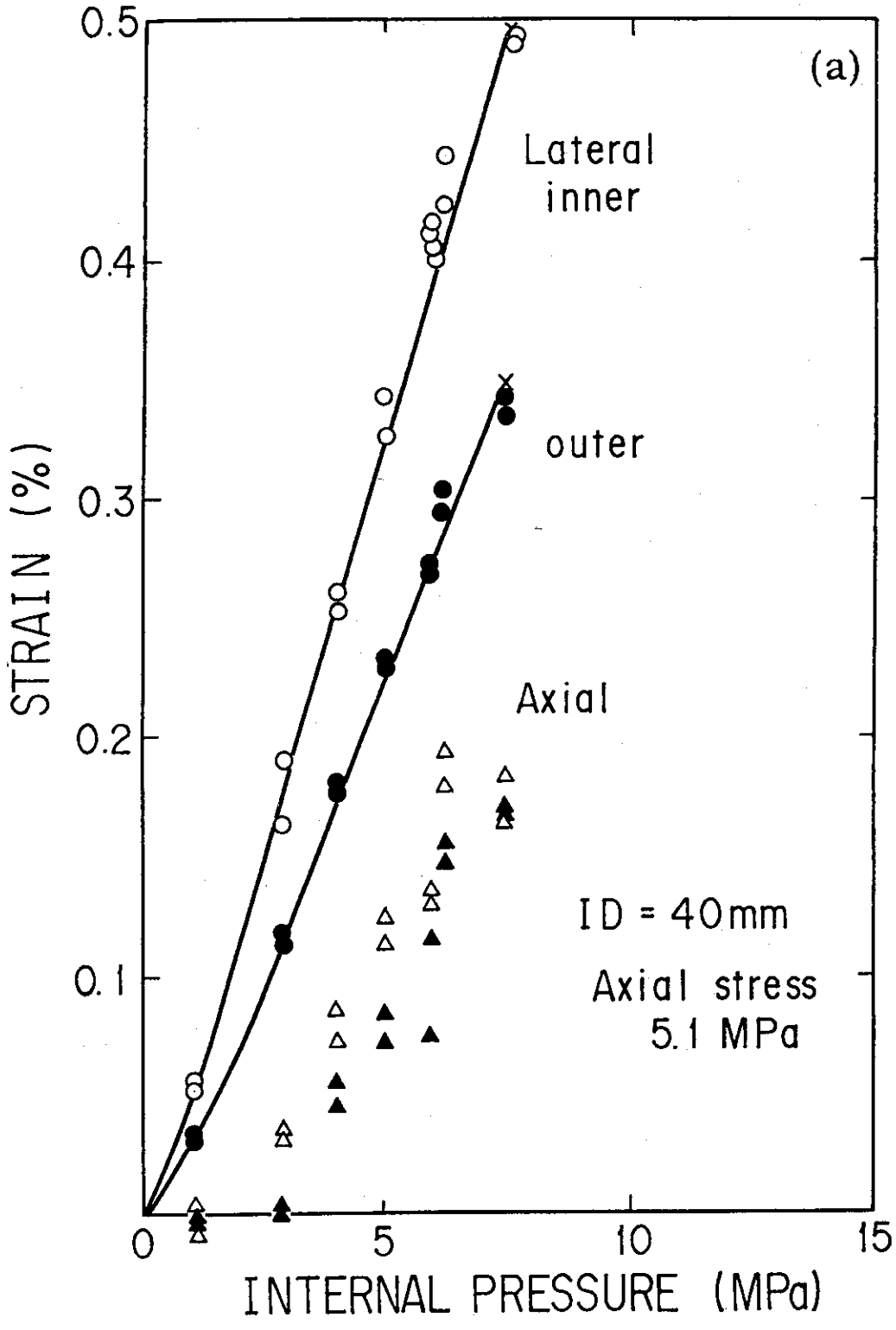

Fig.11 Change in the lateral strain as a function of internal pressure for specimens with 5 mm wall thickness (a) and 10 mm wall thickness (b).

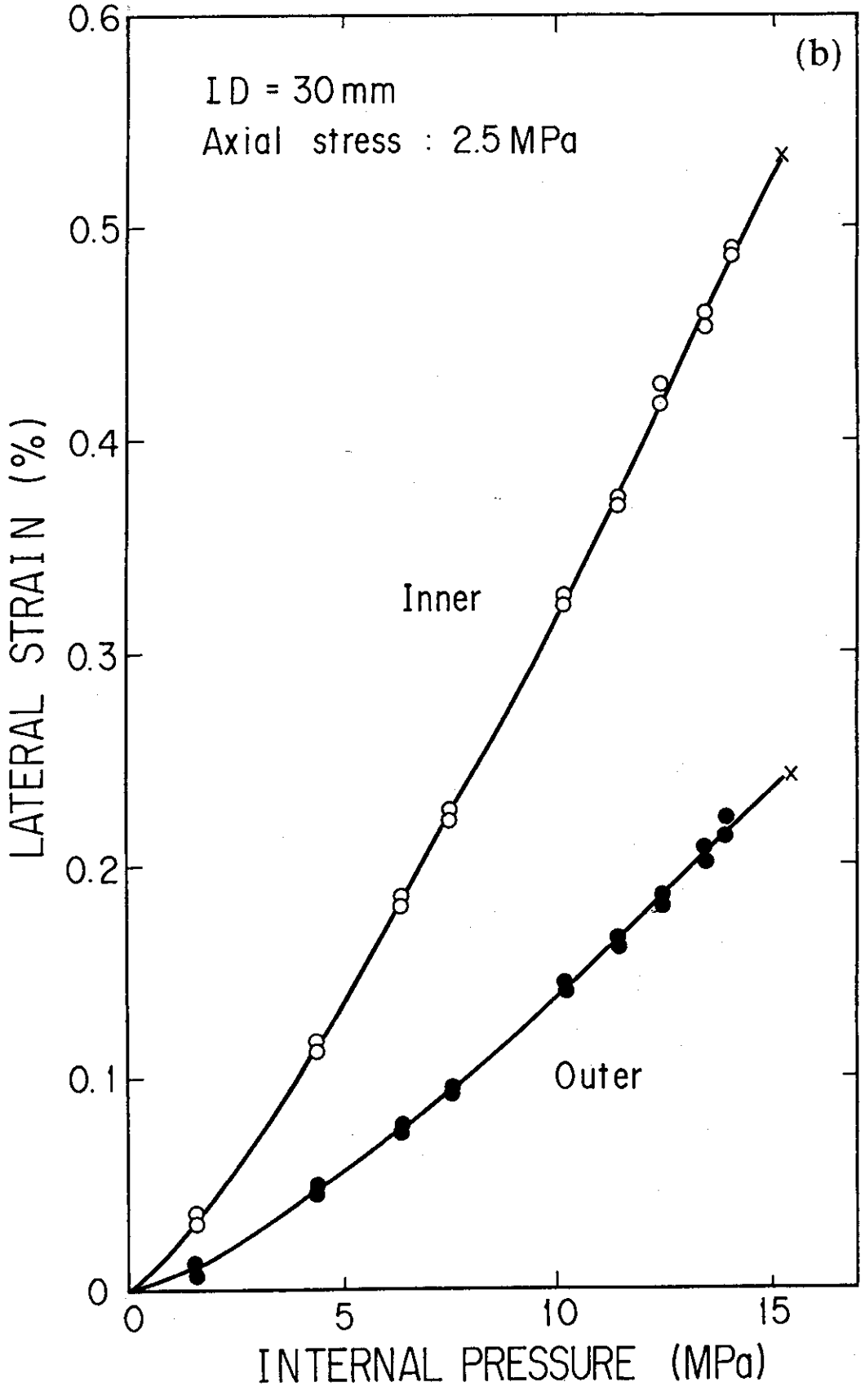

Fig.11 Change in the lateral strain as a function of internal pressure for specimens with 5 mm wall thickness (a) and 10 mm wall thickness (b).

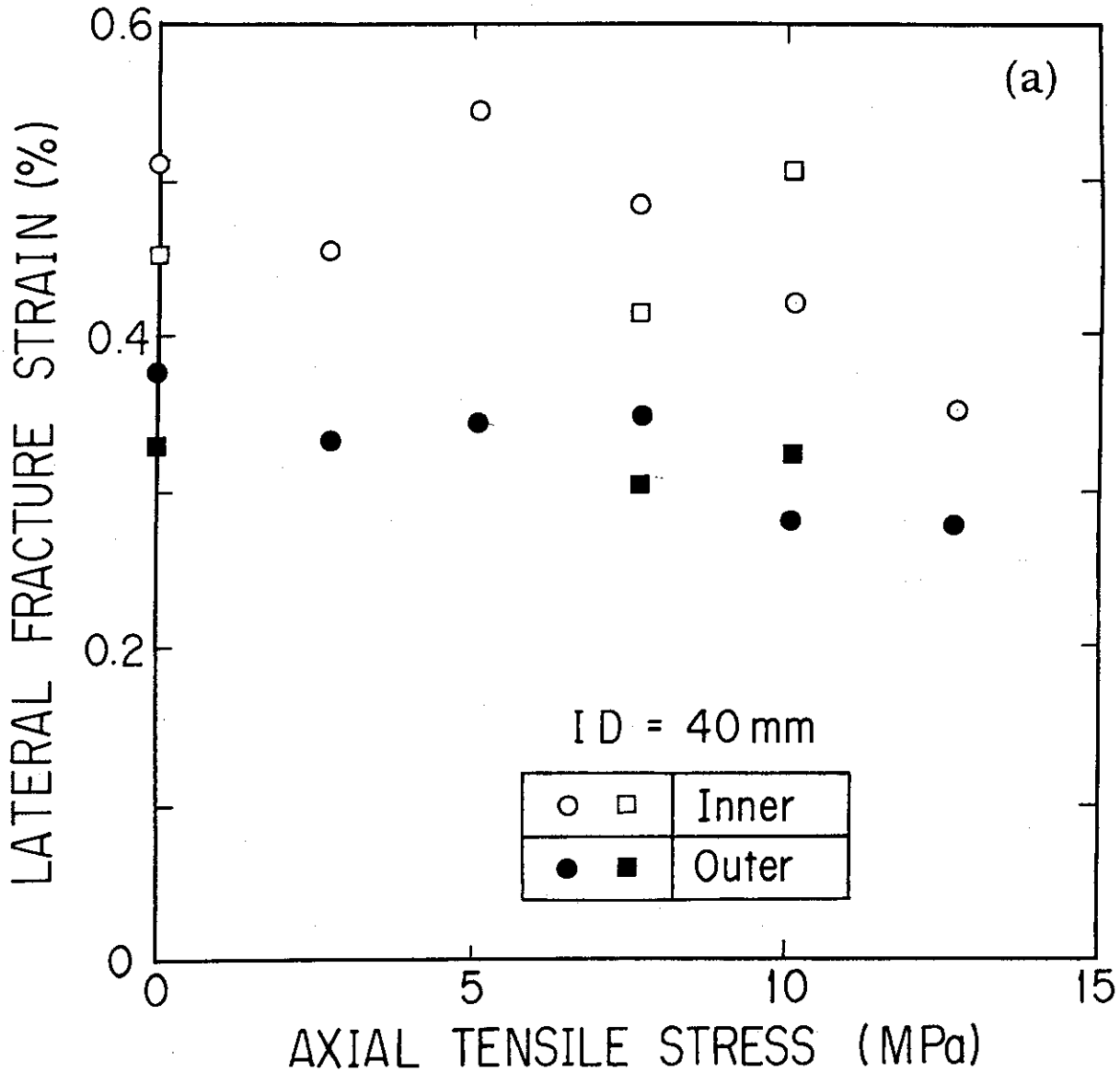

Fig.12 Plots of the lateral fracture strain as a function of axial tensile stress for specimens (a) 5 mm and (b) 10 mm in wall thickness. Here, the open symbols represent the strains at the inner surface, and the solid ones, for those at the outer surface.

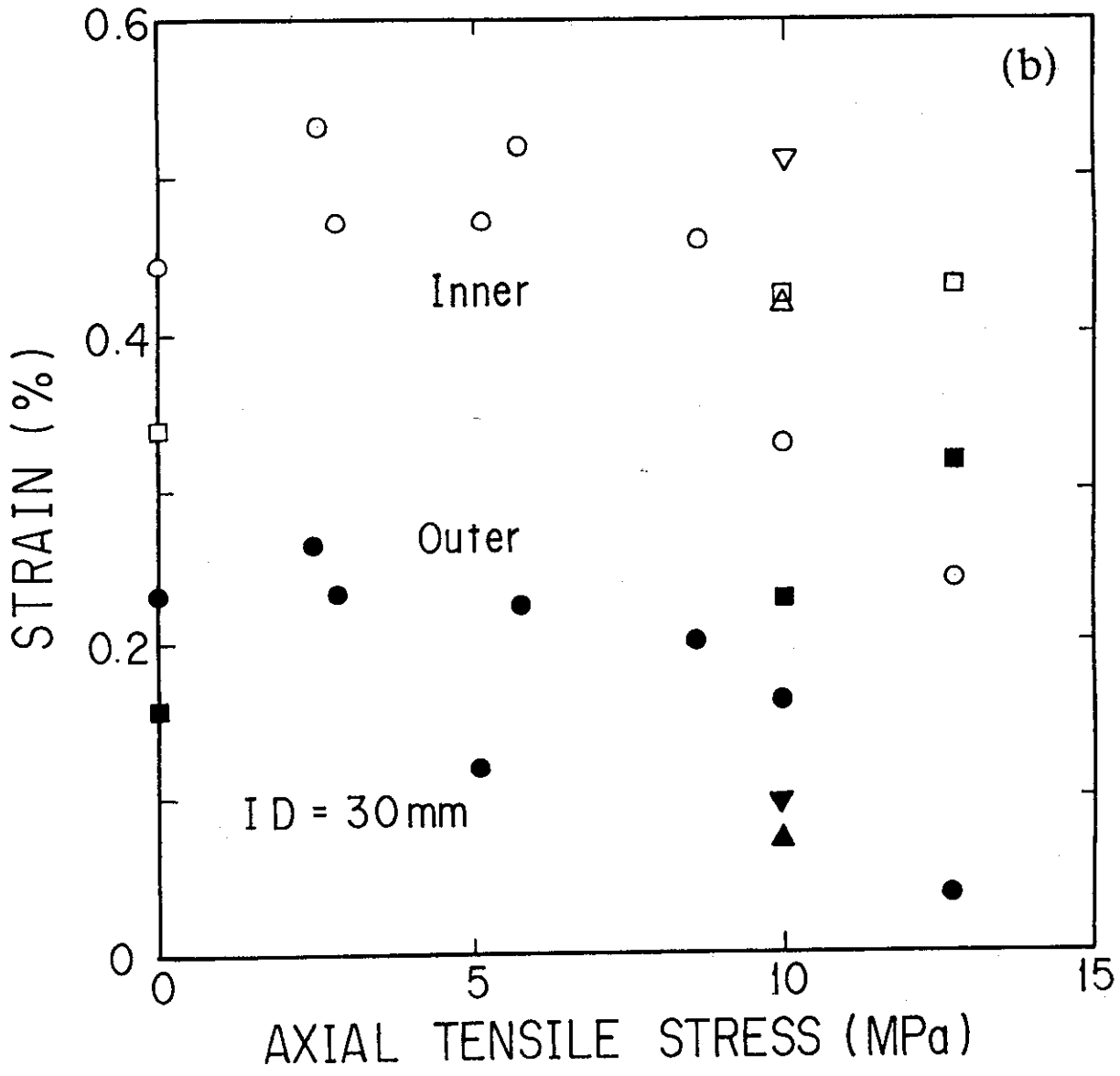

Fig.12 Plots of the lateral fracture strain as a function of axial tensile stress for specimens (a) 5 mm and (b) 10 mm in wall thickness. Here, the open symbols represent the strains at the inner surface, and the solid ones, for those at the outer surface.

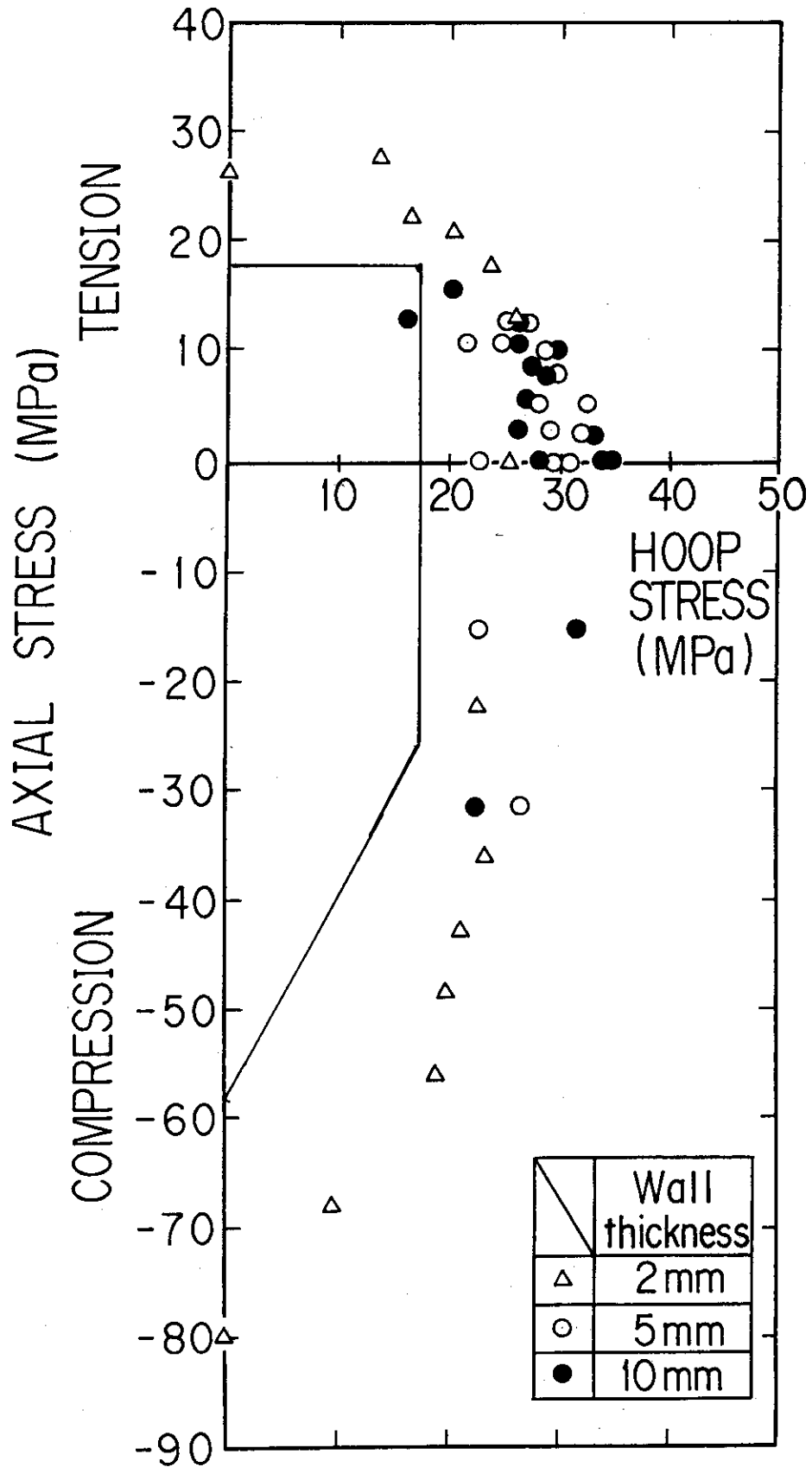

Fig.13 Failure surface data for tubular specimens with different values of wall thickness.

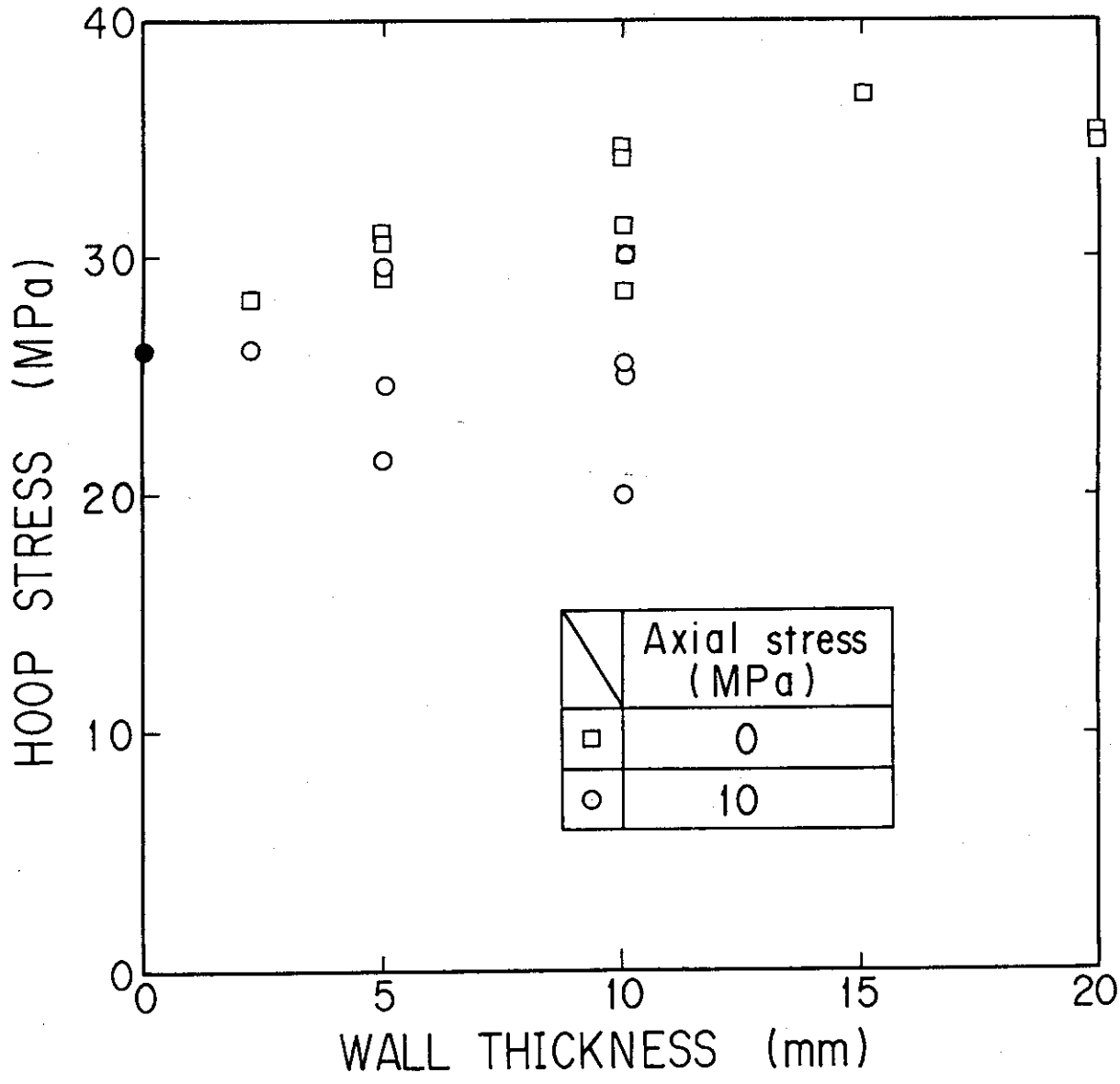

Fig.14 Hoop fracture stress as a function of wall thickness with or without axial stress.

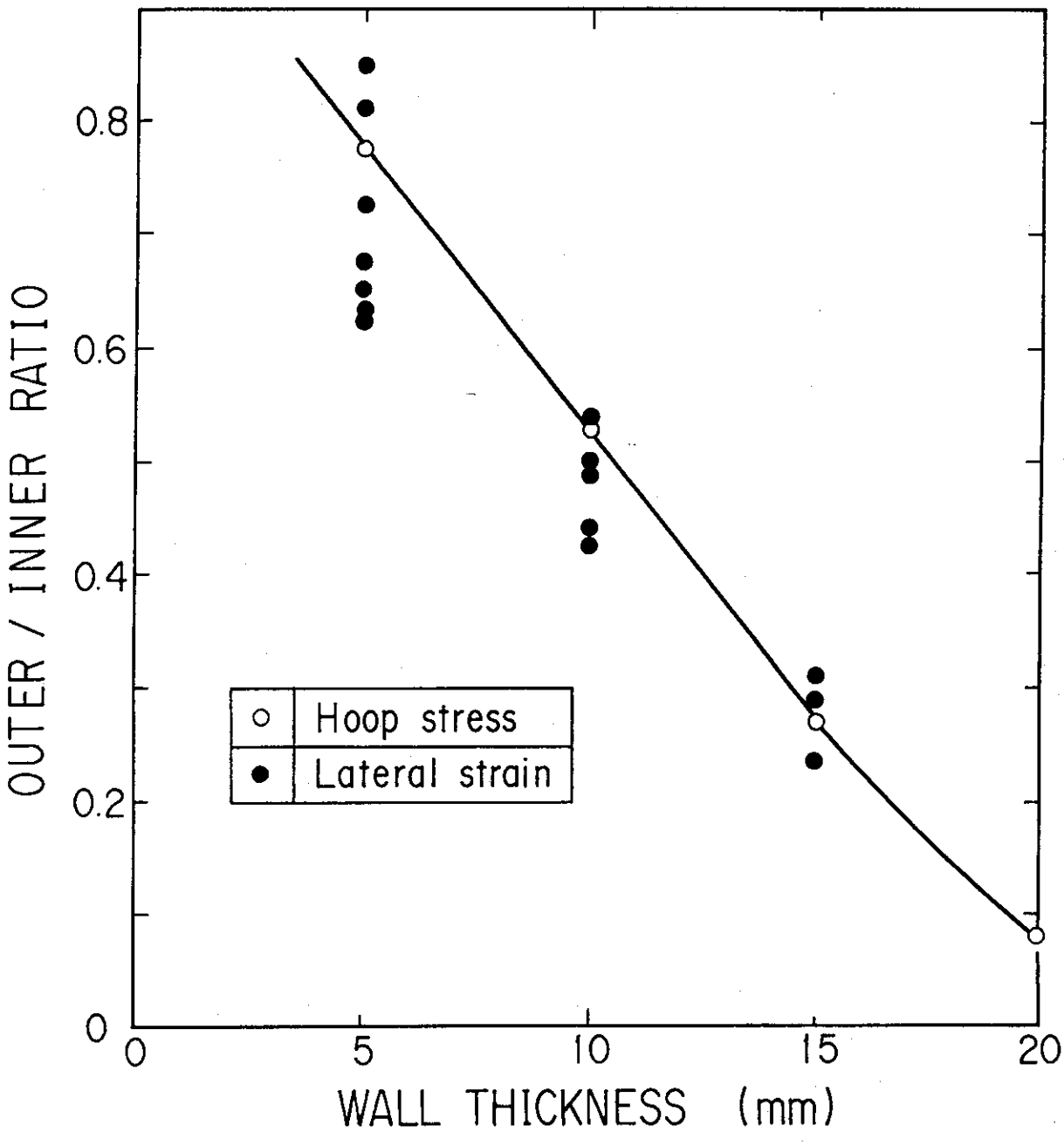

Fig.15 Outer/inner ratios for the hoop fracture stress calculated on the basis of the elastic theory and the lateral strain measured using strain gages.

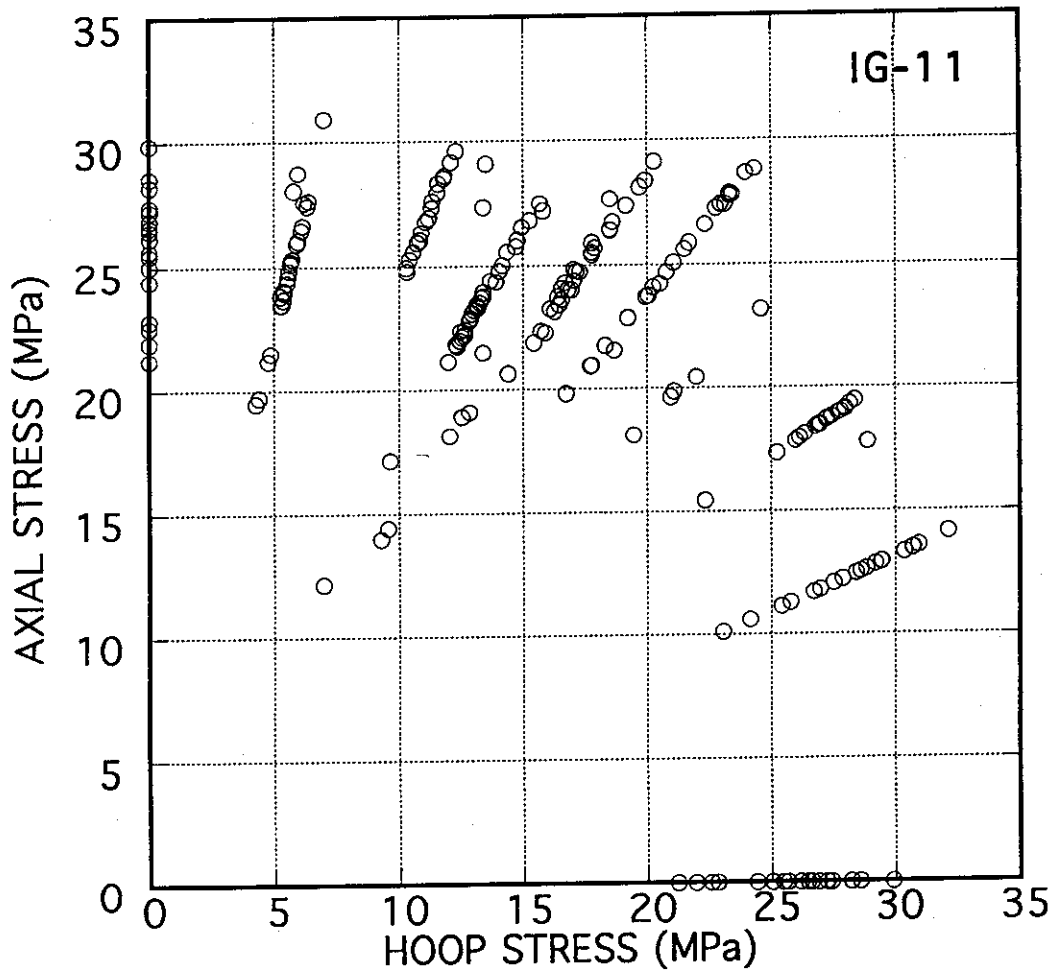

Fig.16 Biaxial strength of IG-11 graphite in the first quadrant of the fracture surface.

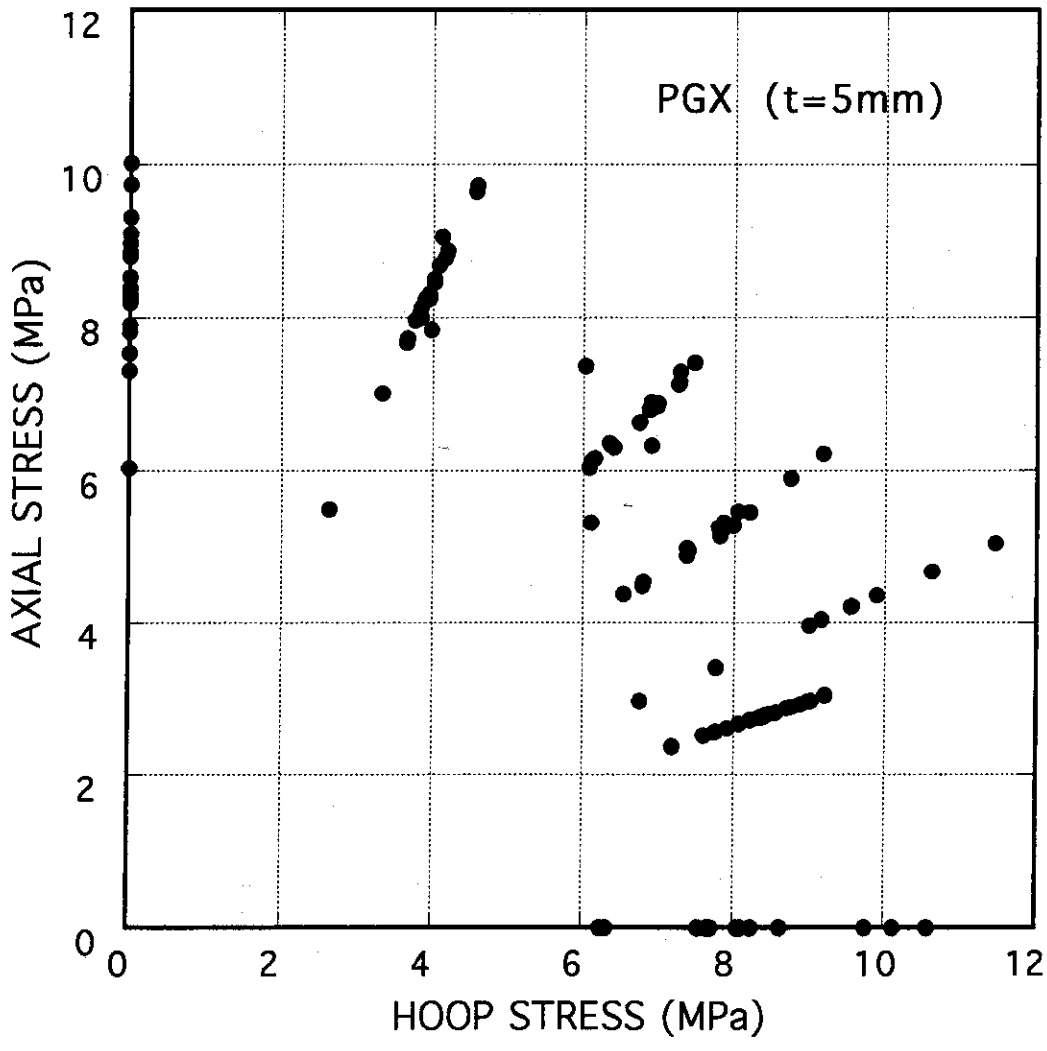

Fig.17 Biaxial strength of PGX graphite in the first quadrant of the fracture surface.

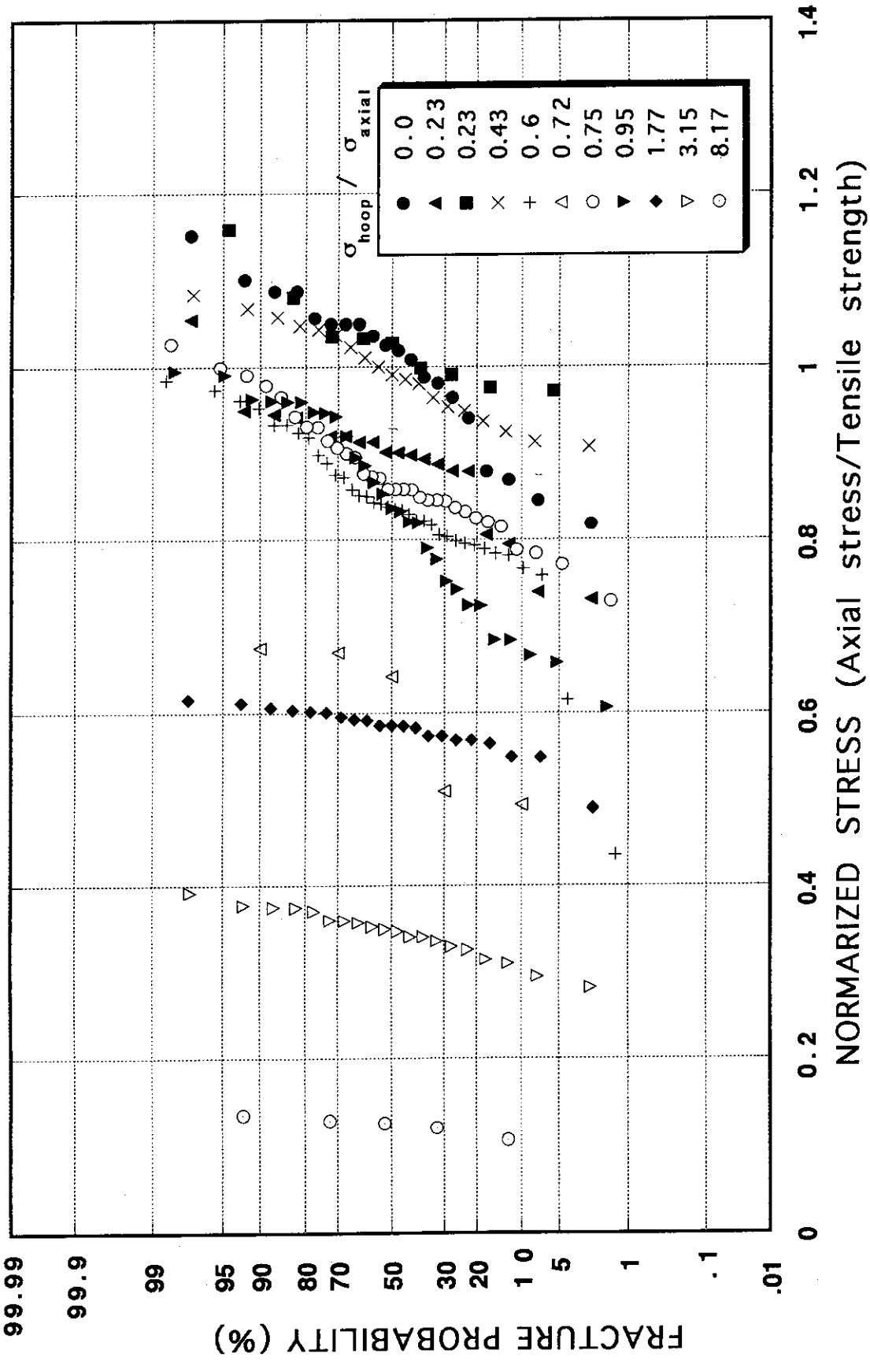

Fig.18 Biaxial fracture probability of IG-11 graphite as a function of normalized axial stress, i.e., axial tensile stress/mean tensile strength,

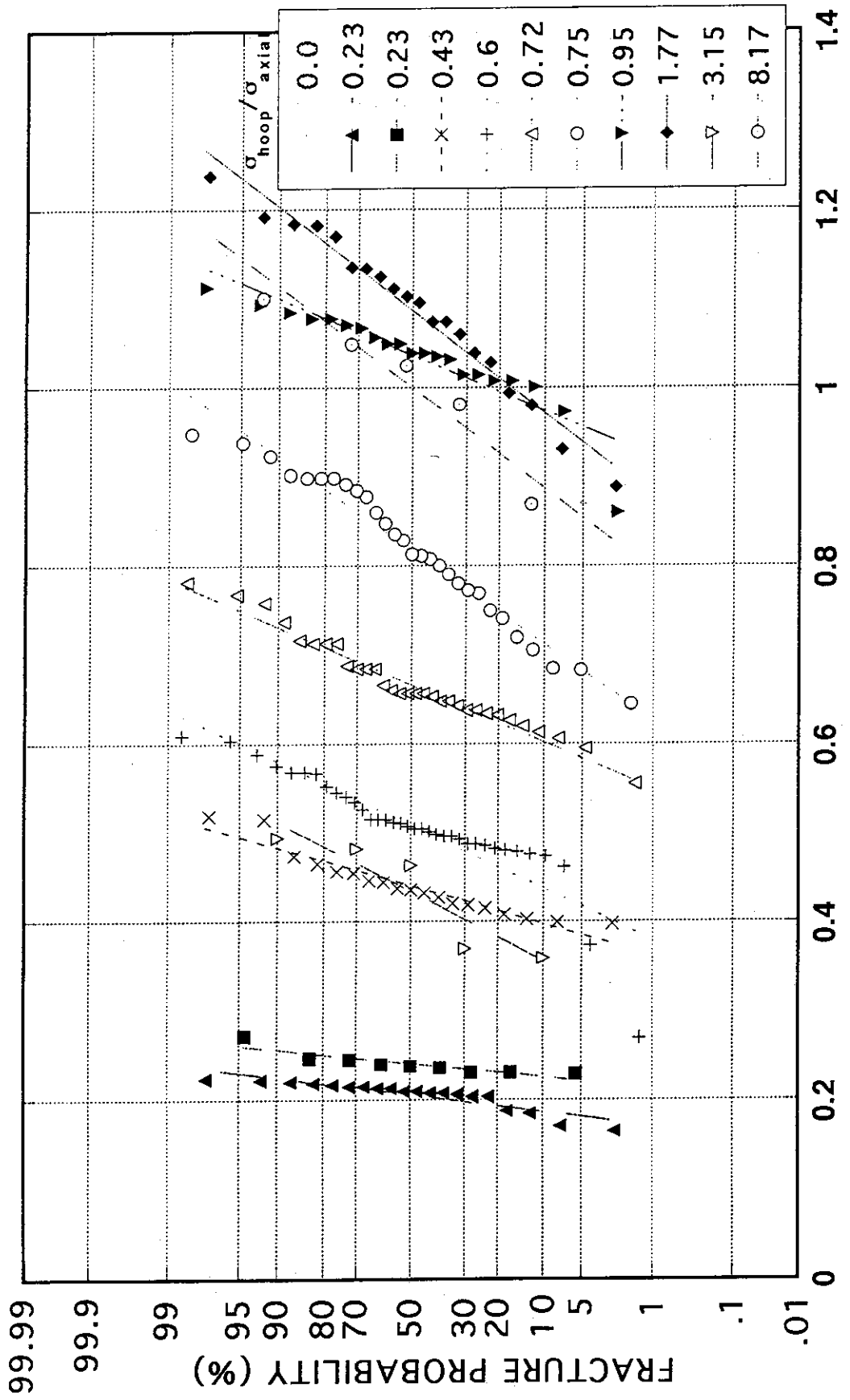

Fig.19 Biaxial fracture probability of IG-11 graphite as a function of normalized normalized hoop stress, i.e., hoop stress/mean tensile strength.

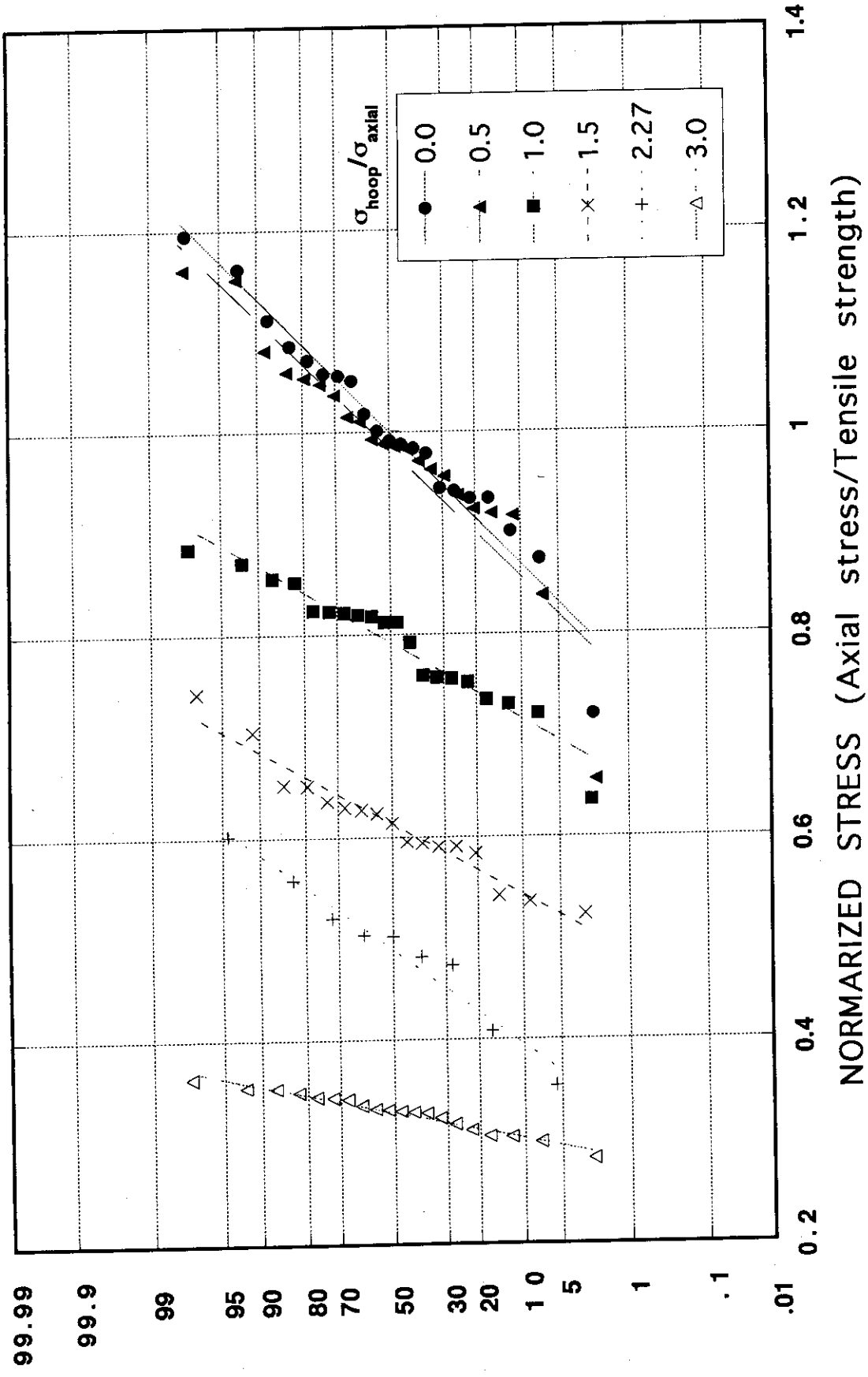

Fig.20 Biaxial fracture probability of PGX graphite as a function of normalized axial stress, i.e., axial tensile stress/mean tensile strength.

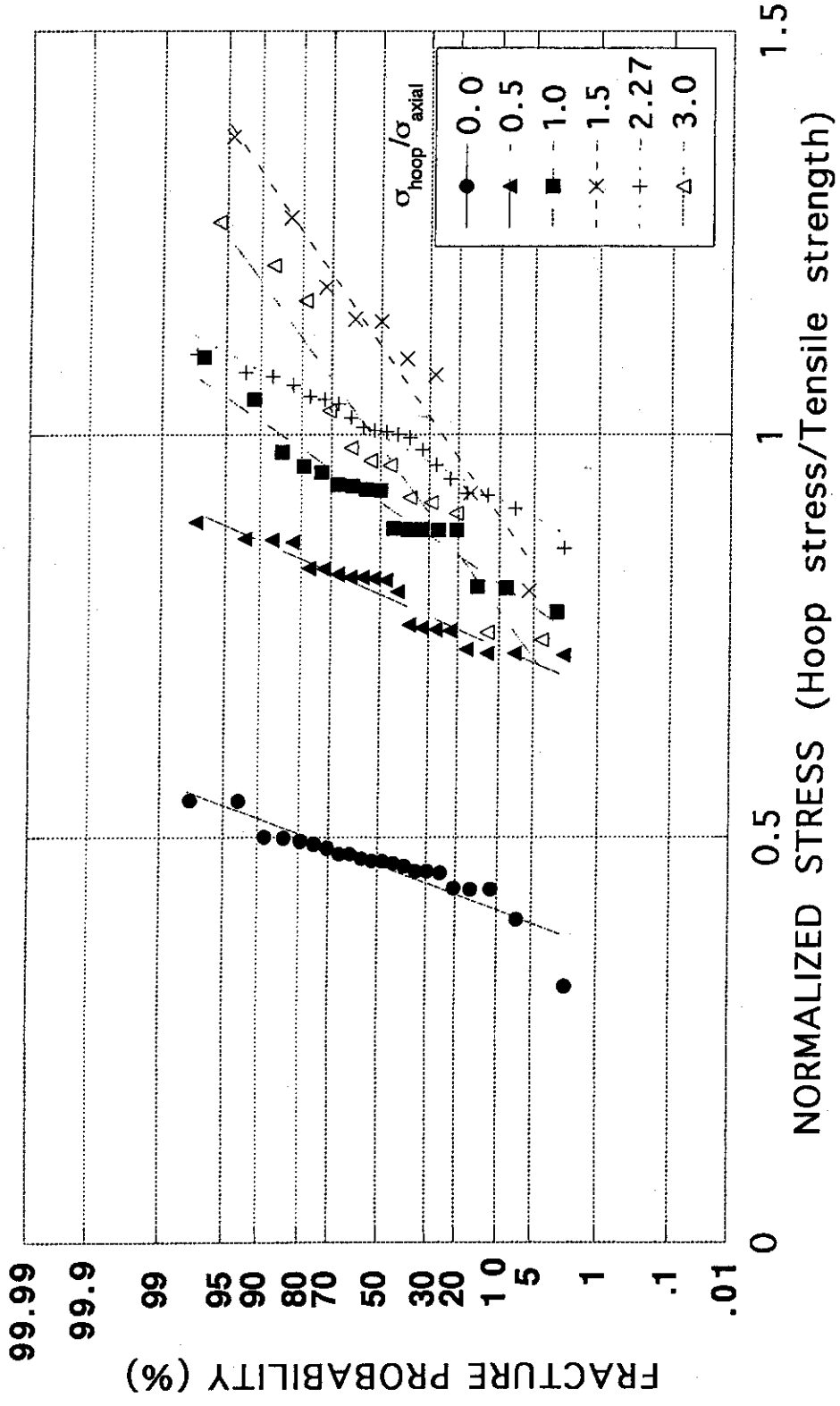

Fig.21 Biaxial fracture probability of PGX graphite as a function of normalized hoop stress, i.e., hoop stress/mean tensile strength.

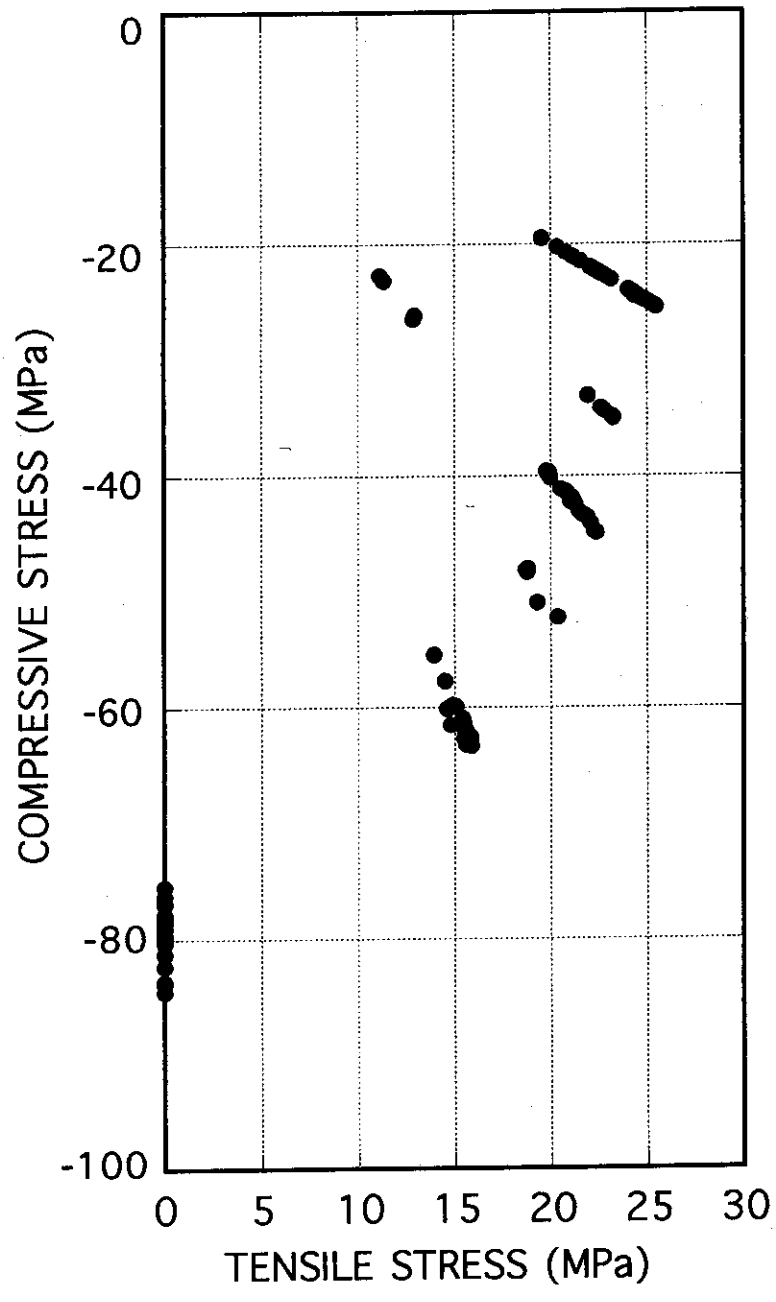

Fig.22 Biaxial strength of IG-11 graphite in the fourth quadrant of the failure surface.

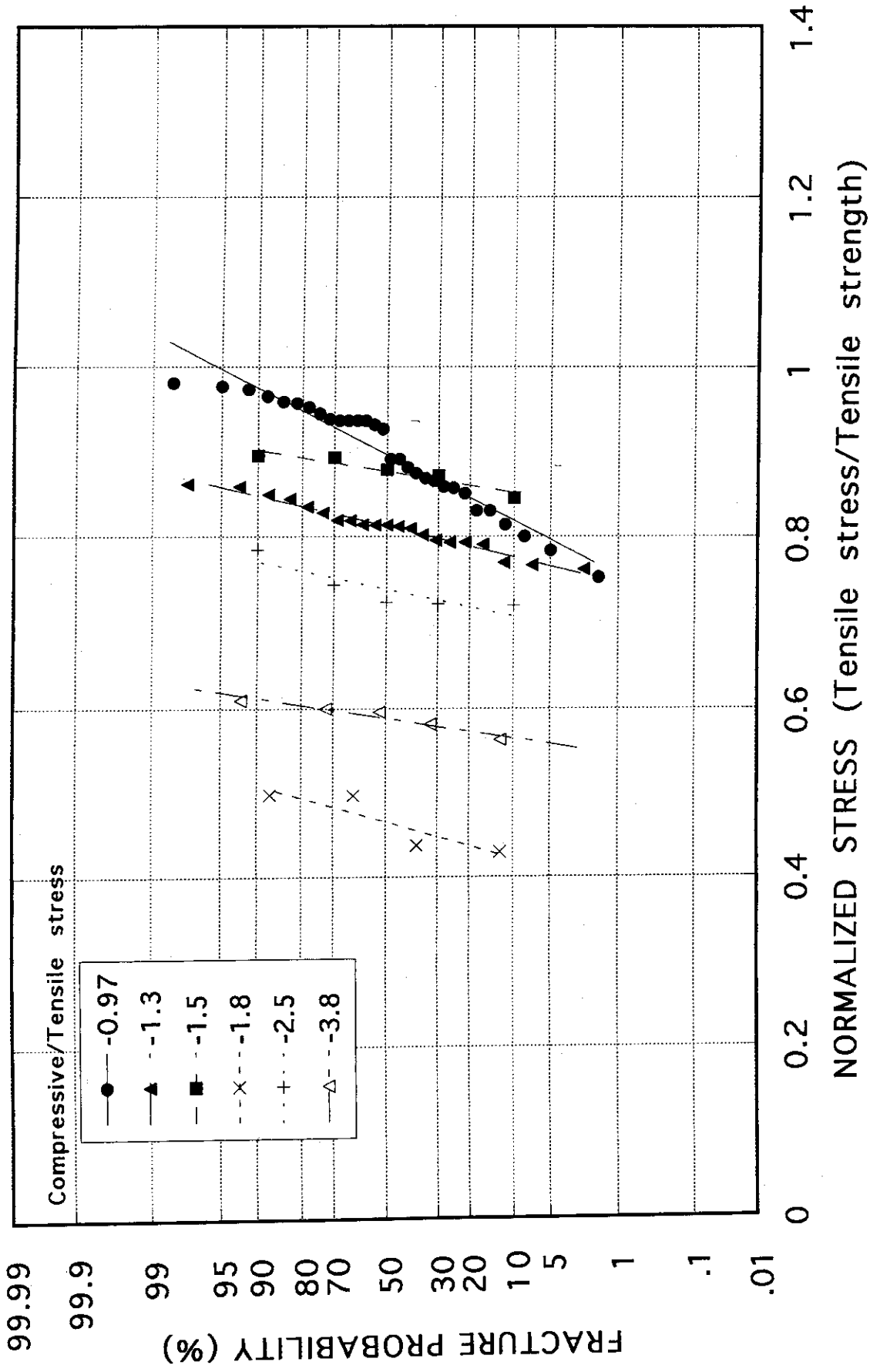

Fig.23 Biaxial fracture probability of IG-11 graphite as a function of normalized circumferential tensile stress, i.e., tensile stress/mean tensile strength.

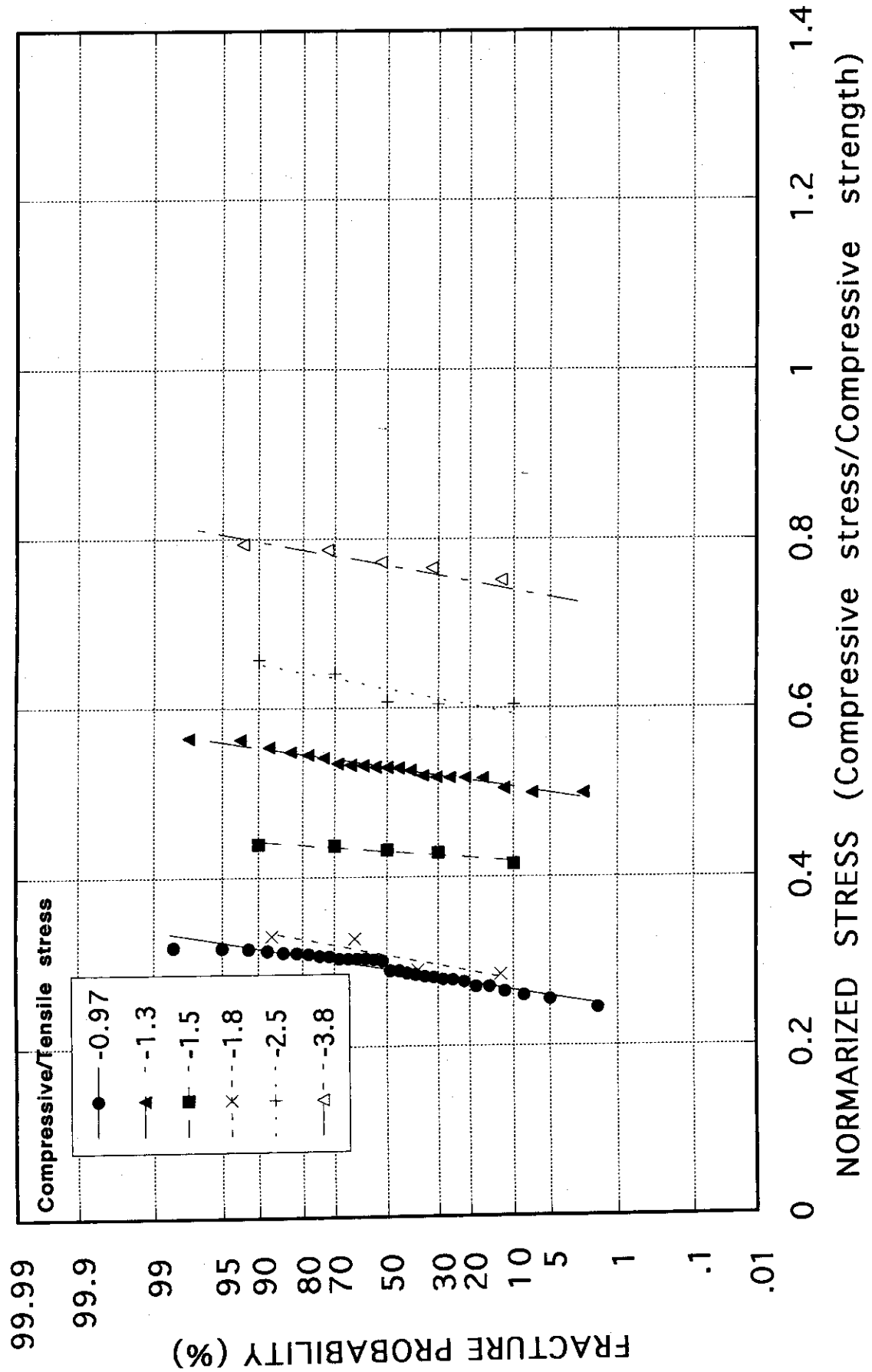

Fig.24 Biaxial fracture probability of IG-11 graphite as a function of normalized axial compressive stress/mean compressive strength.

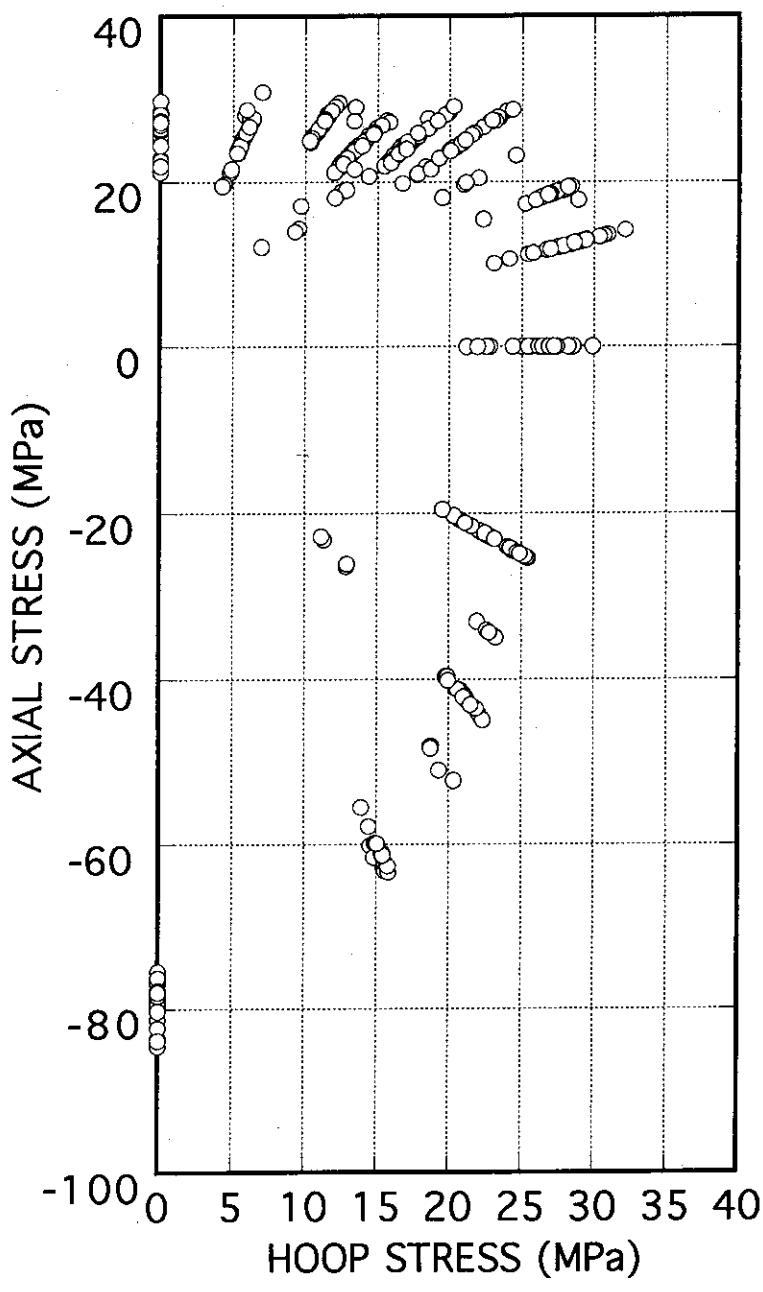

Fig.25 Biaxial strength of IG-11 graphite in the first and fourth quadrants.

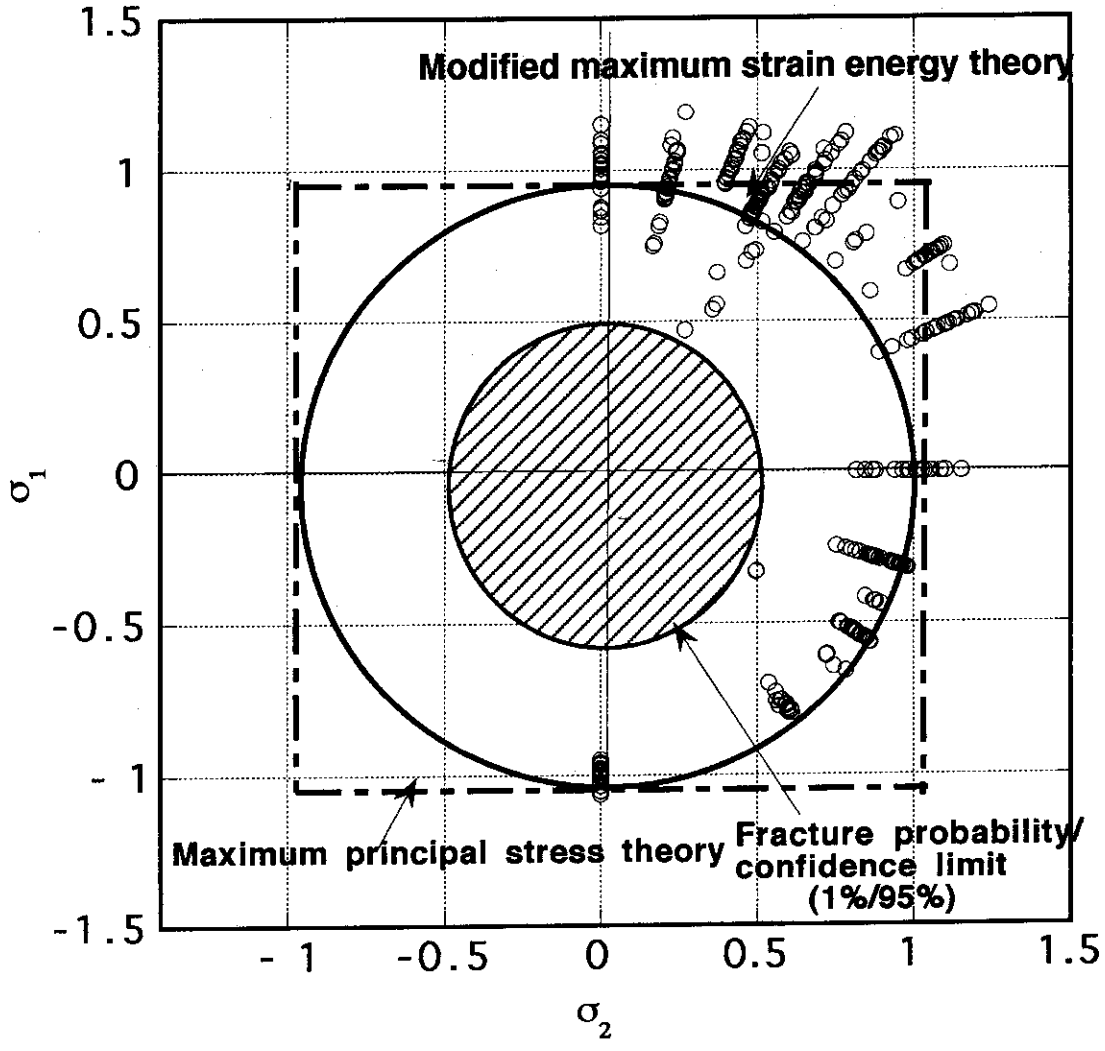

Fig.26 Normalized biaxial strength data for IG-11 graphite, σ_1: axial tensile or compressive stress/tensile or compressive strength, σ_2: hoop or torque tensile stress/tensile strength.

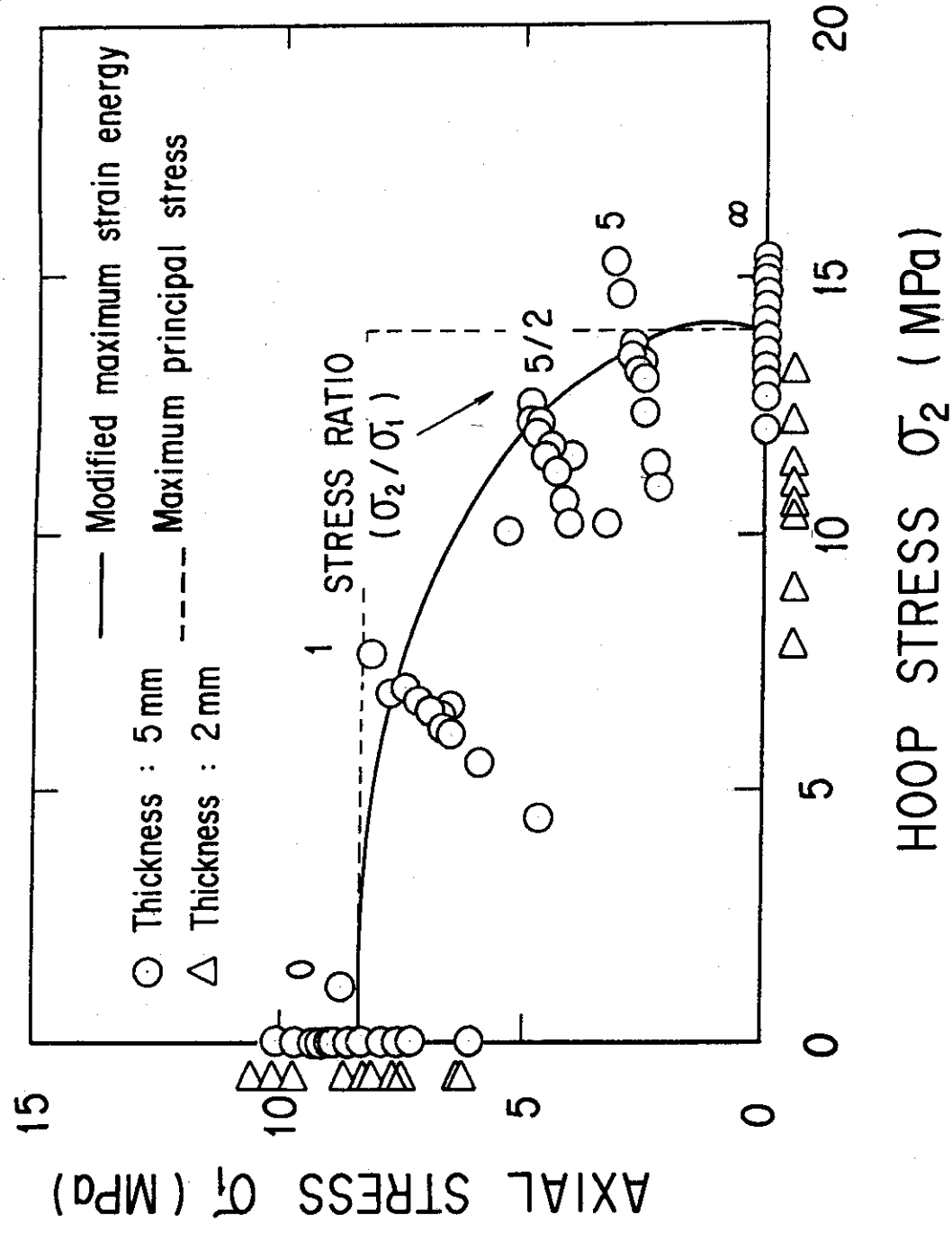

Fig.27 Biaxial fracture strength and fracture criteria for PGX graphite in the first quadrant of the failure surface.

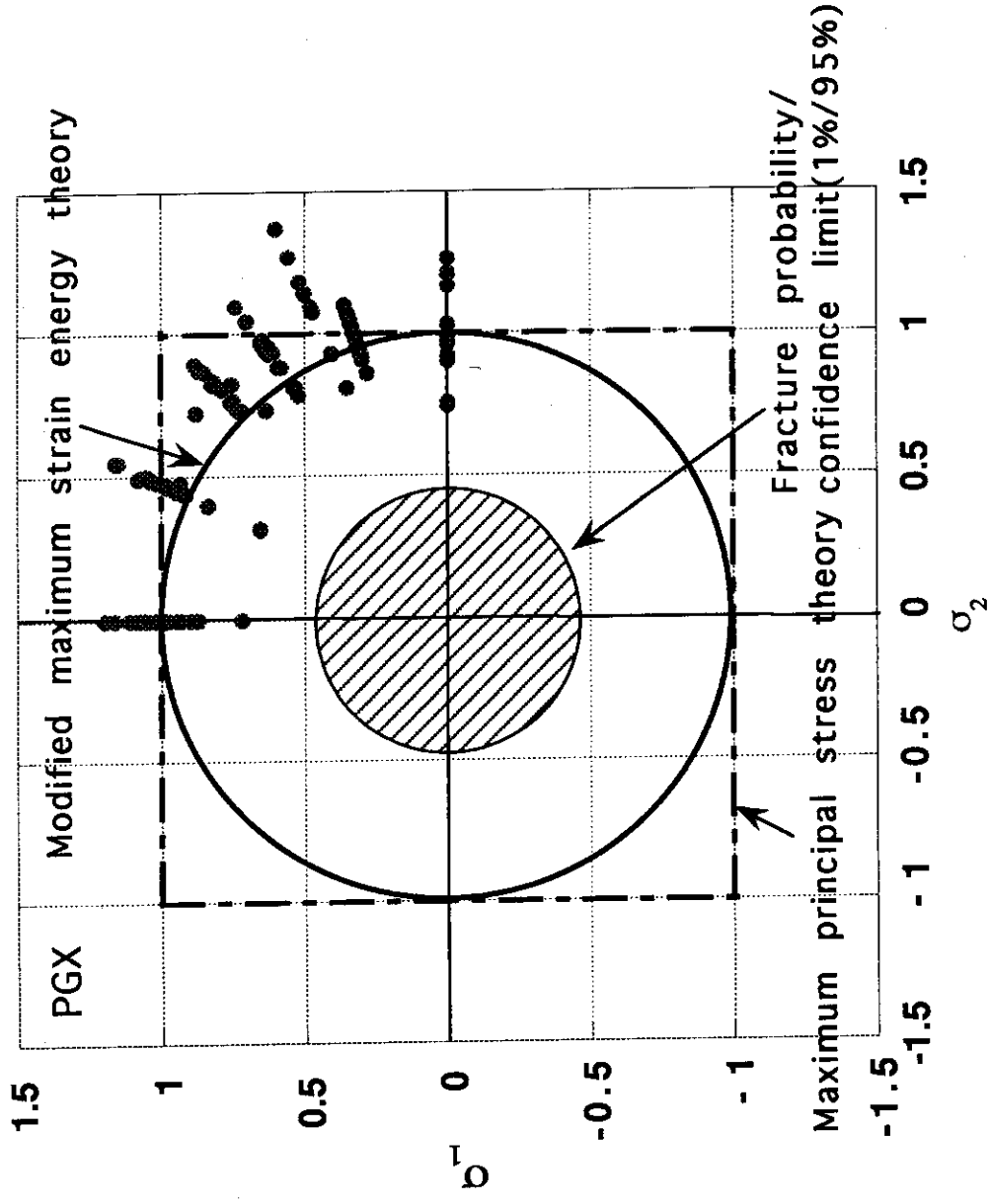

Fig.28 Normalized biaxial strength data for PGX graphite, σ_1: axial tensile stress/tensile strength, σ_2: hoop stress/tensile strength.

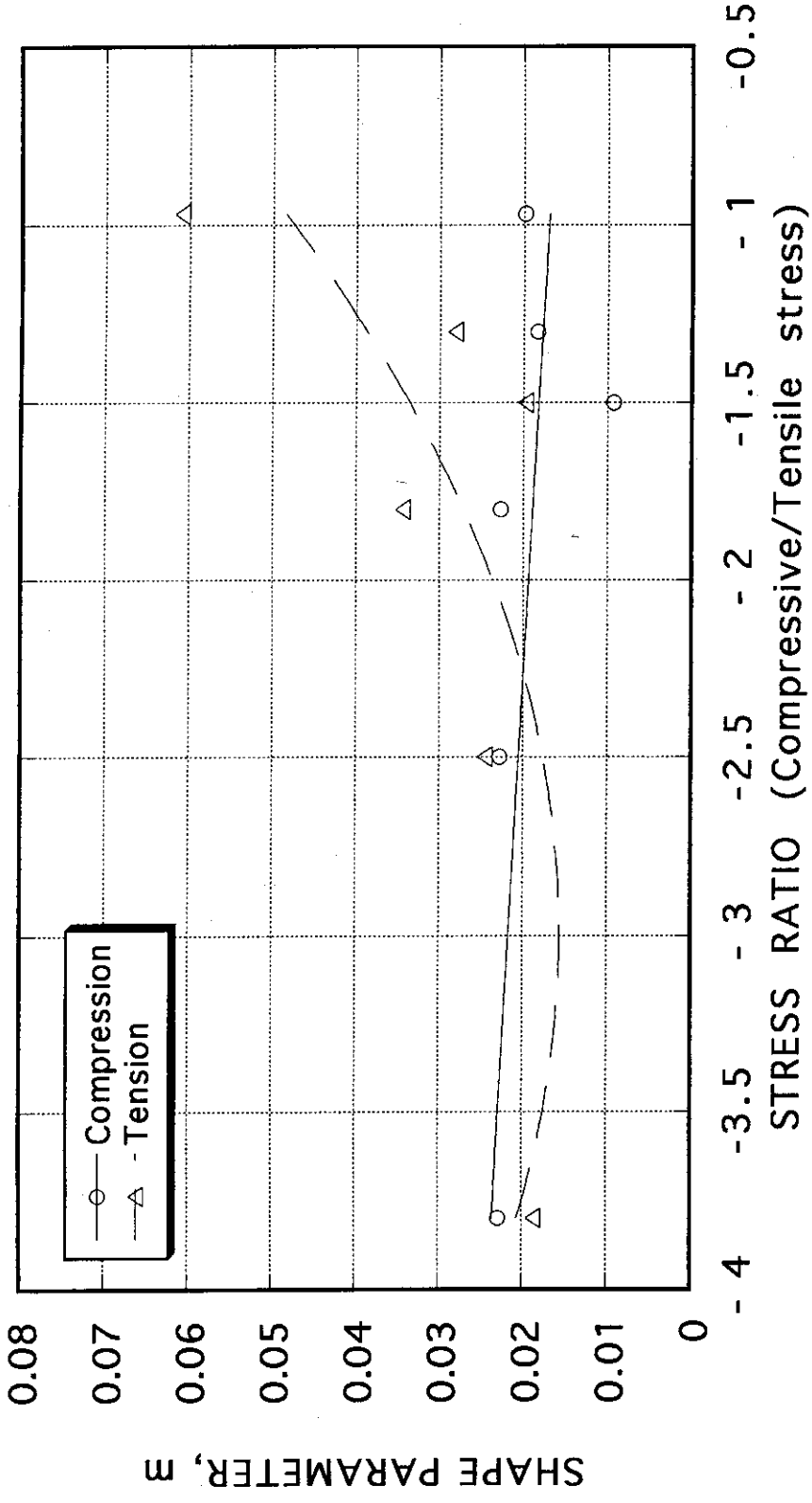

Fig.29 Plots of shape parameter for the fracture data on IG-11 graphite in the fourth quadrant of the failure surface.

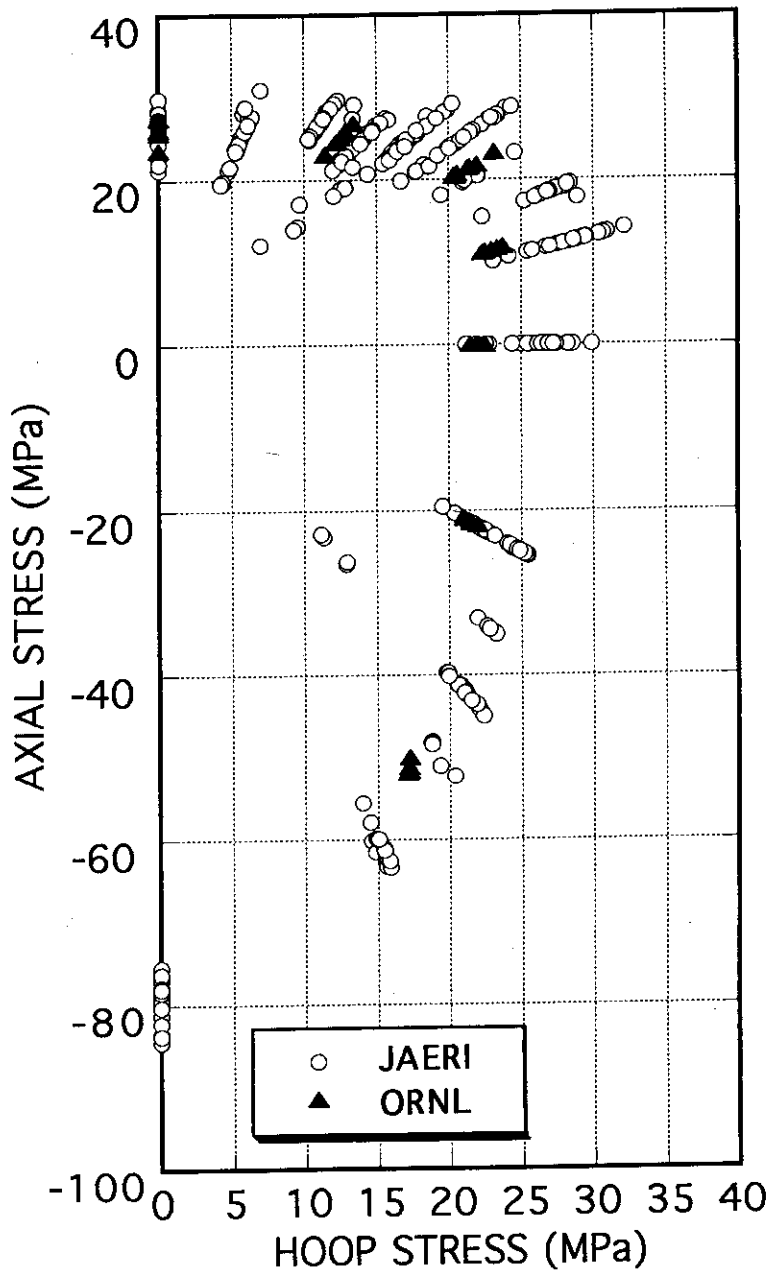

Fig.30 Comparison of JAERI data with ORNL data on the biaxial strength.